RATIONAL DESIGN OF HEMOPROTEINS FOR PEROXIDATION REACTIONS

A Thesis Submitted to
the Graduate School of Engineering and Sciences of
İzmir Institute of Technology
in Partial Fulfillment of the Requirements for the Degree of

MASTER OF SCIENCE

in Bioengineering

by
Gülce GÜRALP

December 2020
İZMİR

ACKNOWLEDGMENTS

Firstly, I would like to express my love and endless thanks to my mother Özlem BİLGİ who always supports me in my life.

I would like to mean the world to my supervisor Assoc. Prof. Dr. Nur Başak SÜRMELİ ERALTUĞ for her guidance, support and comments during my thesis. She always shared valuable information with me during my graduate study and education.

I would like to acknowledge "TÜBİTAK 2210/C Yurt içi Yüksek Lisans Burs Programı-2018" for supporting me financially during my studies. Also, I would like to thank The Scientific and Technological Research Council of Turkey (TUBITAK) 116Z380 grant for supplying financial to this project.

I would like to thank Ekin KESTEVUR DOĞRU for the previous study.

I would also like to thank of Biotechnology and Bioengineering Applications and Research Centre (BİYOMER) for their contributions in my study.

I am grateful to Res. Asst. Melis KÜÇÜKSOLAK for advices, help and comments during my studies, especially HPLC analysis.

I would also like to acknowledge Prof. Dr. Erdal BEDİR, Assoc. Prof. Dr. Ali Oğuz BÜYÜKKİLECİ and Prof. Dr. Çağlar KARAKAYA to allow me utilization of their instruments.

I would like to thank Prof. Dr. Talat YALÇIN for MALDI-TOF/TOF analysis.

Also, I would like to thank Sürmeli Laboratory members; Ekin KESTEVUR DOĞRU, M. Semih BAŞLAR, Alper ŞAHİN, Merve ERDAL and Tuğçe SAKALLI for help and friendship.

I am thankful Fatmanur BOSTAN and Gamze DOĞAN for their precious friendship and encouragement. They always shared both my happy and sad moments.

I would like to thank my office mates; Eyüp BİLGİ, Gülten KURU, Yiğit Ege ÇÖMLEKÇİ, Öykü SARIGİL, Berivan DİZMEN, Göklem ÜNER and M. Ünver KURT for their support in my difficult and exciting times.

Finally, I am grateful to my grandparents Veli BİLGİ and Gülseren BİLGİ, my cousin Yiğit Eren BİLGİ and my uncle Mustafa BİLGİ for their support and endless love.

ABSTRACT

RATIONAL DESIGN OF HEMOPROTEINS FOR PEROXIDATION REACTIONS

Biocatalysts are important for the synthesis of fine chemicals and steroidal drugs in the biopharmaceutical industry. Cytochromes P450 (P450) monooxygenases are significant biocatalysts due to their high selectivity for oxidation reactions. CYP119 is the first characterized thermoacidophilic P450. CYP119 was isolated from *Sulfolobus acidocaldirius*. CYP119 enzyme shows high stability at low pH and high temperature. CYP119 can utilize the peroxidase shunt pathway in the catalytic cycle of P450. These abilities make CYP119 attractive biocatalyst for production of fine chemicals and drugs. In this study, Leu69Gly mutant CYP119 enzyme was cloned by site-directed mutagenesis. L69G and WT CYP119 was expressed successfully in *Escherichia coli* BL21 (DE3) cells with isopropyl β-D-1- thiogalactopyranoside (IPTG). This study shows that L69G mutation is important for binding to progesterone. This was predicted by *in silico* mutagenesis in a previous computational study. Isolation and purification of the WT and L69G CYP119 were carried out. Activity assays and substrate binding studies of the enzymes were performed and compared each other. L69G mutation did not cause significant effect on Amplex Red® oxidation and styrene epoxidation activities. L69G CYP119 (K_S: 34.55 ± 7.4 μM) showed higher affinity for progesterone compared to WT CYP119 (K_S: 69.8 ± 48.9 mM). A new product, thought to be hydroxylated progesterone, was formed as result of hydroxylation of progesterone by L69G CYP119 using peroxidase shunt pathway.

ÖZET

PEROKSİDASYON REAKSİYONLARI İÇİN HEMOPROTEİNLERİN RASYONEL TASARIMI

Biyokatalizörler biyofarmasötik endüstrisinde pahalı kimyasalların ve steroid yapılı ilaçların sentezi için önemlidirler. Sitokrom P450 monoksijenazlar, oksidasyon reaksiyonlardaki yüksek seçiciliklerinden dolayı önemli biyokatalizörlerdir. CYP119 ilk karakterize termoasidofilik P450' dir. CYP119 *Sulfolobus acidocaldirius*' dan izole edilmiştir. CYP119 enzimi düşük pH ve yüksek sıcaklıklarda yüksek kararlılığa göstermektedir. CYP119 P450' lerin katalitik döngüsündeki peroksidaz şant yolağını kullanabilmektedir. Bu yetenekleri CYP119' u pahalı kimyasalların ve ilaçların üretiminde çekici bir katalizör yapmaktadır. Bu çalışmada, Leu69Gly mutant CYP119 enzimi bölgeye yönlendirilmiş mutajenez ile klonlanmıştır. L69G ve WT CYP119, izopropil β-D-l-tiyogalaktopiranosid (İPTG) ile *Escherichia coli* BL21 (DE3) hücrelerinde başarılı bir şekilde ekspres edilmiştir. Bu çalışmalar sonucunda L69G mutasyonunun progesteron bağlanması için önemli olduğu gözlenmiştir. Daha önceki çalışmada bilgisayar ortamında gerçekleştirilen simülasyonlar ile bu mutasyonun progesterone bağlanmasını arttıracağı tahmin edilmiştir. L69G ve WT CYP119 enzimlerinin izolasyonu ve saflaştırması gerçekleştirilmiştir. L69G ve WT CYP119 enzimlerinin aktivite analizleri ve substrata bağlanma çalışmaları yürütülmüştür ve birbiriyle karşılaştırılmıştır. L69G mutasyonu Amplex Red® oksidayonunda ve stiren epoksidayonunda önemli bir etkiye neden olmamıştır. L69G CYP119 (K_S: 34.55 ± 7.4 μM), WT CYP119 (K_S: 69.8 ± 48.9 mM) ile karşılaştırıldığında progesterona daha yüksek affinite göstermiştir. Peroksidaz şant yolağı kullanarak L69G CYP119 ile progesteron hidroksilasyonu gerçekleştirildiğinde yeni bir ürün tespit edilmiştir. Bu ürünün hidroksillenmiş progesteron olduğu düşünülmektedir.

TABLE OF CONTENTS

LIST OF FIGURES

Figure **Page**

Figure **Page**

Figure **Page**

Figure **Page**

LIST OF TABLES

Table **Page**

CHAPTER 1

INTRODUCTION

1.1. Biocatalysis

The utilization of enzymes in chemical synthesis is named as biocatalysis. The enzymes are used by whole cell systems or isolated preparations (Bommarius & Paye, 2013; Truppo, 2017). Biocatalysis is an attractive progress in the pharmaceutical industry and fine chemical synthesis because catalysis with enzymes is highly selective, safe and sustainable. Biocatalysts can contact with the substrate at multiple points thanks to their three-dimensional structures. Properties of biocatalysts can be changed by modifications of the protein sequence. Biocatalysis is an economic and environmental system in contrast to synthetic methodologies (Truppo, 2017). Amongst biocatalysts, cytochrome P450 monooxygenases are attractive green biocatalysts for synthetic applications (McLean et al., 1998; Schulz et al., 2012).

1.2. Cytochrome P450 Monooxygenases

The cytochrome P450 enzymes are a superfamily of hemeproteins (Bernhardt & Urlacher, 2014; Li et al., 2020). P450s are named from the maximum UV-Visible absorption peak at 450 nm when P450 is in the characteristic reduced state and complexed with carbon monoxide (CO) (Cook et al., 2016; Li et al., 2020). The hemeproteins contain heme prosthetic group (iron protoporphyrin IX) (Figure 1.1) (Hrycay & Bandiera, 2012). The coordination of iron of heme pocket to cysteine residue at proximal side of enzyme plays important role in modulating catalytic properties and stability (Mondal et al., 2019).

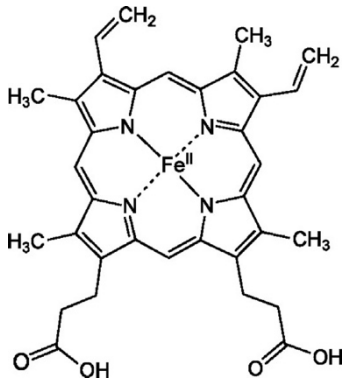

Figure 1.1. Structure of iron protoporphyyrin IX (heme group) (Cook et al., 2016).

P450s are found in human, animals, plants, microorganisms and even viruses (Li et al., 2020). P450s have roles in biosynthesis of steroids, detoxification of xenobiotics, drug metabolism, biosynthetic pathways for natural products and metabolism of fatty acids which are significant for living organisms (Li et al., 2020).

P450 monooxygenases are useful as biocatalysts in biotechnological studies, fine chemical synthesis and biopharmaceutical production because they can react with a wide range of substrates (Koo et al., 2002; Li et al., 2020; Zhang et al., 2014). P450s can catalyze more than 20 different reactions. The reactions include hydroxylation, epoxidation, decarboxylation, N- and O-dealkylation, nitration etc (Li et al., 2020; Rabe et al., 2008; Sakaki, 2012). The substrates of P450 contains terpenoids, polyketides, fatty acids, alkaloids and natural polypeptides. So, P450 enzymes are important catalysts (Bernhardt & Urlacher, 2014; Li et al., 2020). The most significant function of P450 enzymes is to catalyze hydroxylation of C-H bonds regioselectively and stereoselectively. Therefore, P450 enzymes are promising biocatalysts for pharmaceutical, chemical and biotechnological applications (Bernhardt & Urlacher, 2014; Li et al., 2020; O'Reilly et al., 2011).

P450s need redox partners to carry electrons from cofactors in their reactions. This is the problem for industrial applications. Also, other limiting factors of P450s for industrial applications are high cost of cofactors (NAD(P)H etc.), low stability to heat and oxidation and electron uncoupling (Li et al., 2020; Zhang et al., 2014). Also, the inappropriate docking between substrate and active site pocket restricted industrial process (Zhang et al., 2014). P450 enzymes system have been improved with new engineering strategies in recent studies (Li et al., 2020).

1.2.1. Catalytic System of P450s

Catalytic reaction of P450s (Figure 1.2) generally contains the substrate, P450 enzyme, the redox partners and the cofactor. The redox partner serves in electron transfer shuttle and the cofactor supplies the reducing equivalents (Li et al., 2020). P450s use O_2 and two electrons from NAD(P)H as shown in the general formula (Figure 1.2). Redox partners flavoproteins and/or iron-sulfur proteins, mediate electron transfer to the P450s (Hrycay & Bandiera, 2012; Mondal et al., 2019).

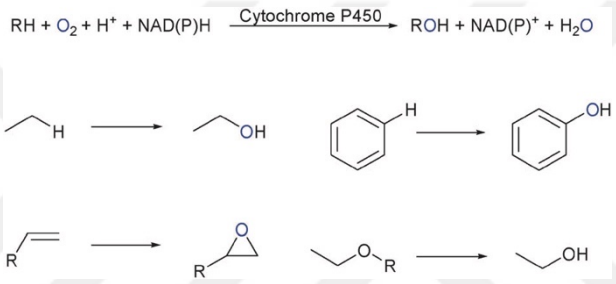

Figure 1.2. Examples of oxidation reactions by P450s. RH shows the substrate and ROH is the product (O'Reilly et al., 2011).

The catalytic system starts with the heme iron of P450 in the ferric resting state bound to distal water (Hrycay & Bandiera, 2012). The heme iron in the ferric resting state of P450 first binds to substrate (RH), which displaces water in the active site of the enzyme. The ferric iron of the high-spin state is reduced to ferrous iron by the first reduction. An electron is supplied from NAD(P)H by redox protein partners. The ferrous iron binds dioxygen and ferrisuperoxo complex is formed via oxygen binding. The second electron is transferred to generate dinegatively charged ferriperoxo complex. One of the negative charges is on oxygen while the other is over the cysteine ligand. The ferrihydroperoxo intermediate (Compound 0) is generated by addition a proton to distal oxygen. As a result of O-O bond cleavage in Compound 0 by addition of the second proton, the water molecule is released and the high-valent porphyrin π radical cation tetravalent iron referred as Compound I, a highly reactive complex is formed. The ferryl-hydroxo intermediate (Compound II) is formed by removing hydrogen atom from substrate via Compound I. The hydroxyl group in Compound II reacts with radical of

substrate and the hydroxylated product is produced. Lastly, the water molecule binds to the ferric heme in resting state in consequence of releasing of the product (Hrycay & Bandiera, 2012; Li et al., 2020).

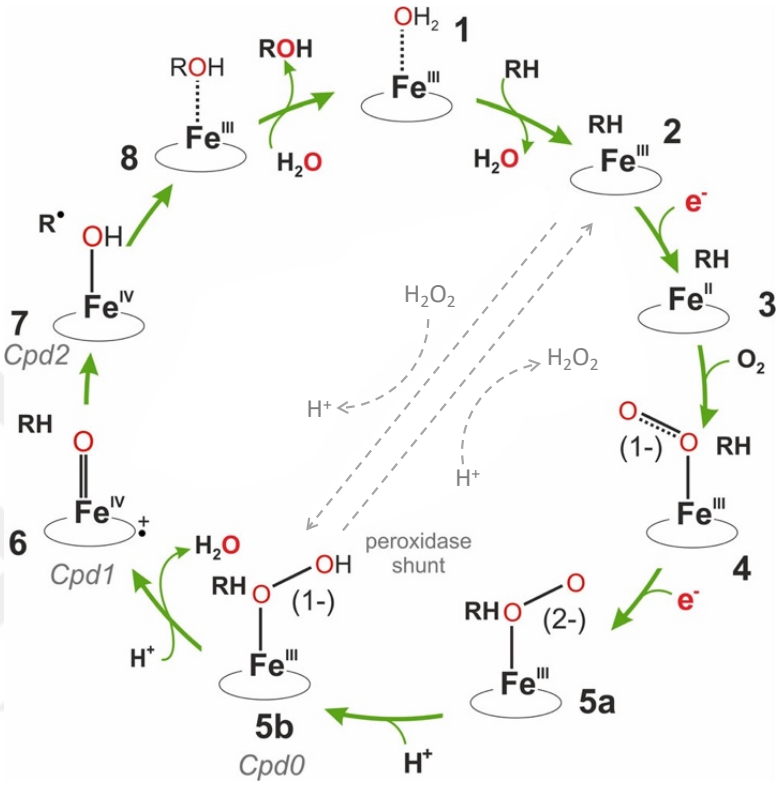

Figure 1.3. Catalytic system of P450s (Szaleniec et al., 2018).

Redox partners play role in electron transfer in the catalytic system of P450s. P450 systems are classified according to types of redox partners and their relationships. There are five classes of P450 systems. FAD-containing ferrodoxin reductase (FdR) and small iron-sulfur-containing ferrodoxin (Fdx) are used in the Class I P450 system. Most of bacterial and mitochondrial P450s has the Class I. Cytochrome P450 reductase (CPR) is used in the Class II P450 system which are employed by eukaryotic organisms. In the Class III P450 system, CPR is fused to C terminus of P450 via flexible linker. The Class IV P450 systems have FMN/Fe_2S_2-containing reductase fused to P450. Directly interaction between P450 and its electron donor occurs in the Class V. These P450s are $P450_{Nor}$ and P450 TxA (Figure 1.4) (Li et al., 2020).

Another way for P450s to catalyze oxidations without the need redox partners, is utilizing hydrogen peroxide (H_2O_2) as an oxidant to form Compound I. The pathway is called as peroxide shunt pathway. This pathway allows P450s catalyze reactions without using redox partners. But the some of P450s shows low tolerance towards H_2O_2. This situation negatively affects efficiency of P450s with H_2O_2 as substrate (Li et al., 2020; Shoji & Watanabe, 2014).

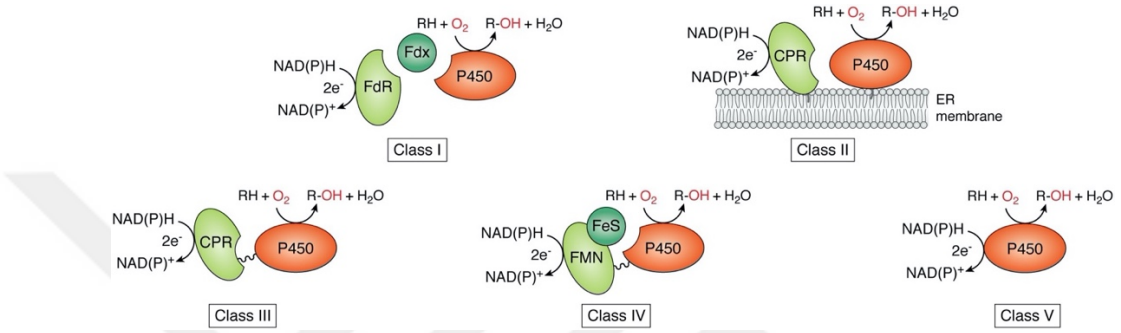

Figure 1.4. Redox partner proteins of P450s (Li et al., 2020).

1.2.1.1 Shunt Pathway

Eliminating the need for NAD(P)H or electron transfer proteins in P450s, will lead to the range of applications of P450 enzymes in the industry. Some P450s can utilize peroxides such as hydrogen peroxide, cumene hydroperoxide and *tert*-butyl hydroperoxide as the active oxygen sources. This reaction is called as shunt pathway (Sakaki, 2012). In H_2O_2-shunt reaction, the ferric heme iron reacts directly with peroxide following by heterolytic cleavage of O-O bond. Compound I forms, which is a highly reactive intermediate. Compound I is responsible for monooxygenation. But sometimes H_2O_2-shunt reaction is inefficient and the enzyme is rapidly inactivated (Cirino & Arnold, 2002; Shoji & Watanabe, 2014). In this process, other peroxides including cumene hydroperoxide and *tert*-butyl hydroperoxide can also be used (Shoji & Watanabe, 2014).

1.2.2. Applications of P450s

Variety of substrates and reaction types of P450s provides numerous applications for pharmaceuticals and chemicals production, biosensors, bioremediation, biodegredation and chemoenzymatic synthesis (Li et al., 2020; Sakaki, 2012).

Catalysis bioconversion from compactin in *Penicillium citrinum* to pravastatin by P450sca-2 (CYP105A3) was reported by Watanabe et al. This process is performed by fermentation by *Streotpmyces carbophilus*. Pravastatin is a potent low-density lipoprotein (LDL)-chlesterol-lowering drug (Sakaki, 2012; Watanabe et al., 1995). Another application of P450s is the actinomycete P450-dependent bioconversion from vitamin D_3 to 1α,25-dihydroxyvitamin D_3 (1α,25$(OH)_2D_3$). 1α,25$(OH)_2D_3$ is a significant drug for osteoporosis, hypothyroidism and chronic renal failure (Sakaki, 2012).

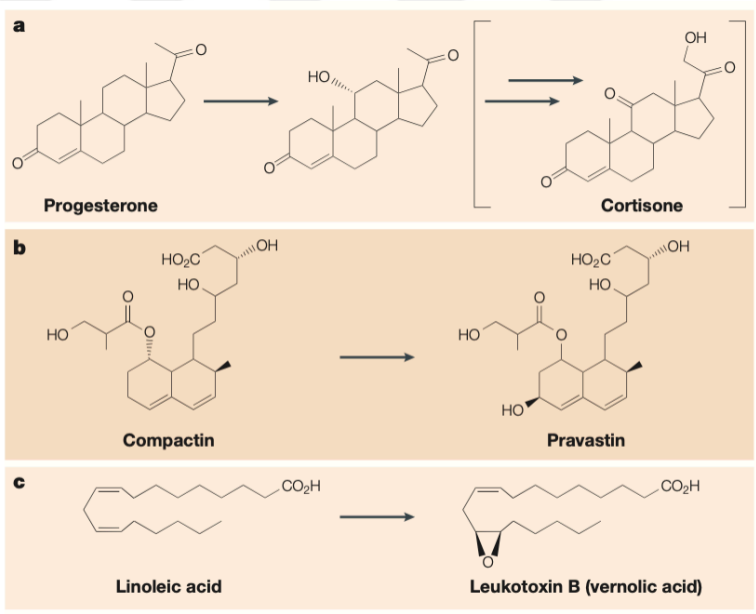

Figure 1.5. Cytochrome P450 reactions used to synthesize drug (Guengerich, 2002).

A biosensor based on the redox properties of CYP3A4 was developed by Joseph et al. CYP3A4 was adsorbed on polycation layer and this film was assembled on gold electrodes. When CYP3A4 substrates containing verapamil, midazolami quinidine and

progesterone were added to oxygenated solution, the reduction current in cyclic voltametric and amperometric experiments increased by dependent concentration. Biosensors can be utilized to identify drugs (Sakaki, 2012).

Bioremediation technologies have also been developed for soils and sediments contaminated with industrial chemicals like dioxins. P450 enzymes are found in dioxin-metabolizing enzymes. Studies by Sakaki & Munetsuna reported that mammalian P450s can degrade mono-, di-, and tri-chlorodibenzo-p-dioxin (CDD) (Sakaki, 2012).

1.2.3. Limitations for P450s Applications of P450s

P450s have some limitations for commercial applications although their potential is high. These limitations contain low activities and difficulties in protein design studies, required for electron transfer partners, problems in the electron transfer and need of NAD(P)H. Also, other problems can appear when bioconversion is performed in whole-cell systems. They are consuming of NAD(P)H, solubility and toxicity of substrate or product and intaking of substrates and product flow from the cells (Bernhardt & Urlacher, 2014; Koo et al., 2002; O'Reilly et al., 2011).

1.3. CYP119: Thermophilic P450 Enzyme

CYP119 is the first characterized member of the thermophilic cytochrome P450 enzymes (Puchkaev et al., 2003; Rabe et al., 2008). CYP119 gene was cloned from *Sulfolobus acidocaldirius* (Zhang et al., 2014). Initially, the source of CYP119 was misidentified, *Sulfolobus solfataricus* (Rabe et al., 2008). *Sulfolobus* species which are archaea that can adapt to two extreme extremes including high temperature (75-80 ºC) and low pH (pH 2-5), found in sulfurous volcanic hot springs (Figure 1.6.B) (Koo et al., 2000). Therefore, *Sulfolobus* spp. and their thermoacidophilic enzymes are interest of industrial application with harsh process conditions. CYP119 has shown thermostability and barostability (Koo et al., 2002; McLean et al., 1998). After expression of CYP119 in

E. coli and purification, the molecular structure was identified by X-ray crystallography (Zhang et al., 2014).

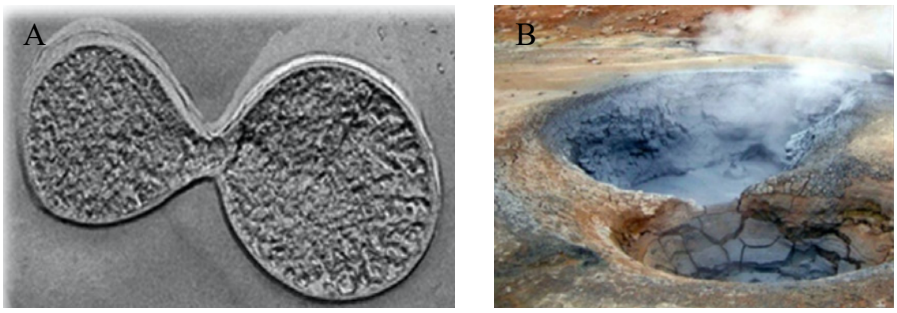

Figure 1.6. *Sulfolobus acidocaldirius* (A). Volcanic hot springs where *Sulfolobus acidocaldirius* was isolated (B).

CYP119 has 368 aminoacids (Puchkaev et al., 2003). Primary structure of CYP119 has recognizable features (Figure 1.7). First, CYP119 is a soluble protein because CYP119 lacks hydrophobic tail. Second, the heme binding region of CYP119 is highly identical to mammalian, fungal and bacterial P450s. Third, the conserved cysteine in the heme coordination and highly conserved threonine are found in CYP119 and are important for activation (Koo et al., 2000).

The natural redox partners and the natural substrates of CYP119 are not known. CYP119 can catalyze the hydroxylation of lauric acid and the epoxidation of styrene (Koo et al., 2002; Puchkaev et al., 2002). The catalytic activity of CYP119 was measured by using Amplex Red® (Rabe et al., 2008). The electrochemical reduction of nitrite, nitric oxide and nitrous oxide and the electrochemical dehaloganation of from CCl_4 to CH_4 are carried out by CYP119 (Blair et al., 2004; Immoos et al., 2004; Rabe et al., 2008). Compound I is formed by CYP119 through peroxide shunt in catalytic system of P450 thanks to the rigid active site structure. This makes CYP119 attractive to use in the industrial applications (Zhang et al., 2014).

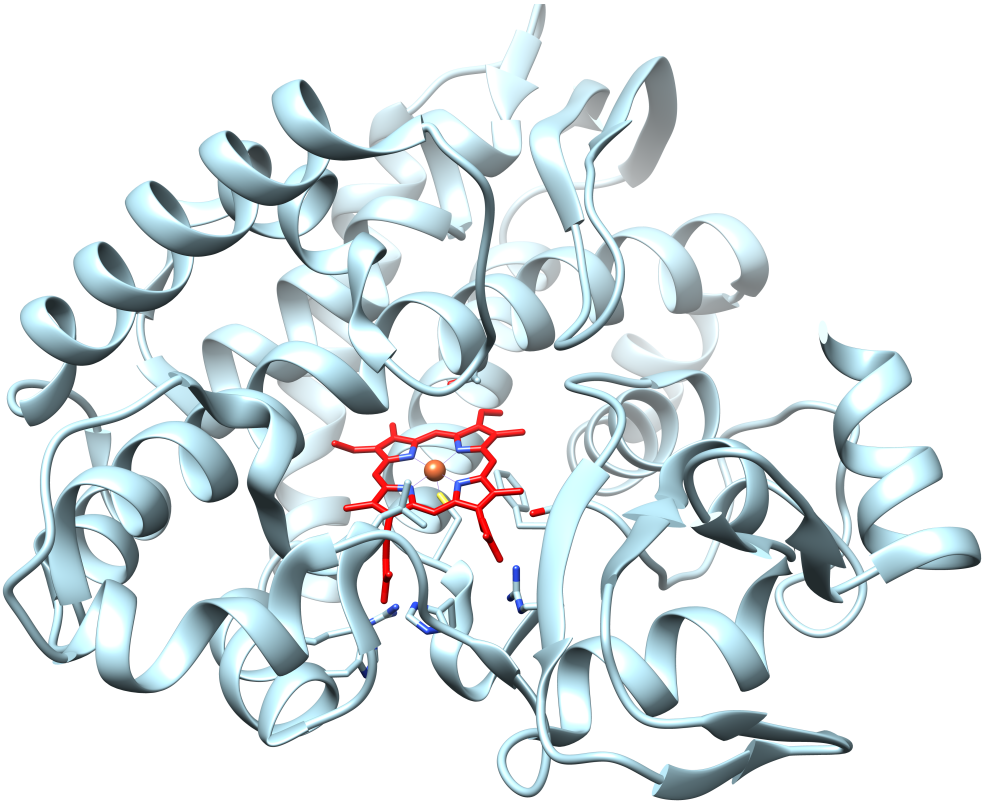

Figure 1.7. Crystal structure of CYP119 illustrated by UCSF Chimera.

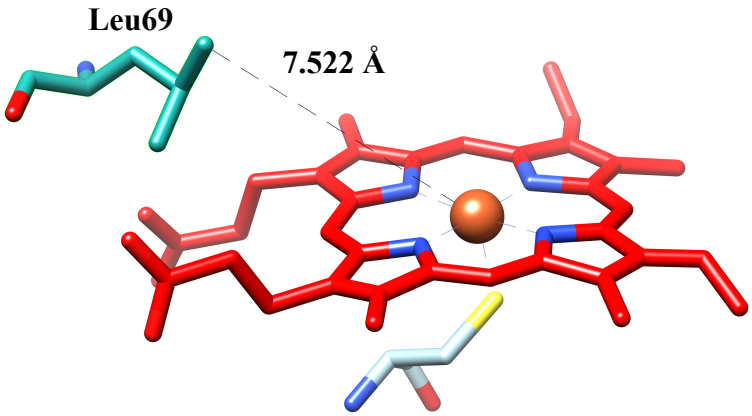

Figure 1.8. Distance of Leu69 residue to heme iron. Image by UCSF Chimera.

1.4. Steroids

Steroids are largely utilized as important molecules in medicine. Combination methods of chemical and microbial conversion has been developed for industrial production of steroids (Sakaki, 2012).

Steroidal compounds are terpenoid lipids. Steroids have four central rings. Variety of specific physiological activities was obtained by differences of functional groups attached to the carbons in the rings and structural modifications (Szaleniec et al., 2018). Steroids are found in animals, plants and microorganisms. Cholesterol, testosterone, progesterone and cholic acid are common steroids. Many steroids are significant drugs used for treatment of diseases including steroidal sex hormones for treatment of male sexual organ dysfunctions, eczema, asthma and Addison' s disease and improvement of protein metabolism and hypotensive activity. Structural modifications on steroids can provide bioactivity, solubility and stability of action.

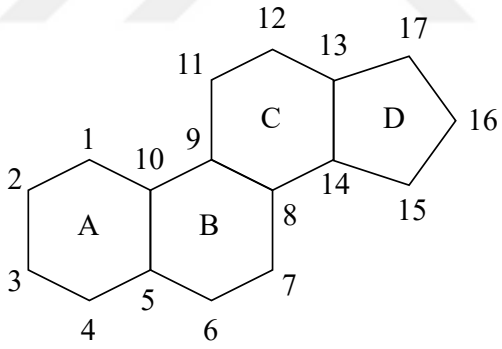

Figure 1.9. Steroid core and the numbering of carbon atoms in the central rings.

In 1950's, the development of steroid drugs started with the identification of the 11α-hydroxylation activity of *Rhizopus* species, in fungi.

The microbial biotransformation of P450s is one of the most successful process for the production of steroid drugs. Reduction, hydroxylation, esterification, methylation, halogenation and methoxylation are types of steroid conversions. Hydroxylation is one of the most useful and cost-effective conversion types to synthesize intermediates of some

steroid drugs. The 11α-, 11β- and 16α-hydroxylations are especially significant because they have applications in the industrial steroid drug production. Many of the steroid hydroxylases are P450 monooxygenases (Szaleniec et al., 2018).

1.4.1. Progesterone and Progesterone Derivatives

Progesterone is a sex hormone for women; structure of progesterone is shown in Figure 1.10. Progesterone has positive effects on the health of women. During ovulation period, progesterone is produced. Progesterone is important molecule for synthesis of another steroids like cortisone (Di Renzo et al., 2020; Sundström-Poromaa et al., 2020). Each progesterone derivative has a special function.

11α-hydroxyprogesterone is a significant pharmaceutical product. This product has an anti-androgenic activity with minimum estrogenic and progestational side effects. 11α-OH-progesterone affects the blood pressure regulation by selective inhibition of 11β-hydroxysteroid dehydrogenase type 2 which metabolizes from cortisol to cortisone in humans. So, 11α-OH-progesterone can be utilized for formation of cortisone and hydrocortisone (Nikolaus et al., 2017).

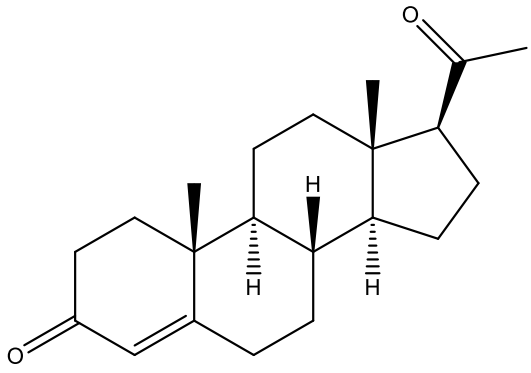

Figure 1.10. Structure of progesterone.

6β- hydroxyprogesterone and 9α-hydroxyprogesterone also have pharmaceutical importance. 6β- hydroxyprogesterone is an intermediate for the synthesis of 6β, 14α-

dihydroxyandrost-4-ene-3,17-dione which is an inhibitor for the growth of breast cancer cells. 9α-hydroxyprogesterone is used as an intermediate in the synthesis of substances which show glucocorticoid and progestational activity. Biotechnological synthesis is useful for production of 6β- hydroxyprogesterone and 9α-hydroxyprogesterone (Nikolaus et al., 2017).

1.5. Improvement of P450s

In modern biotechnology, the use of enzymes and engineered enzymes by mutagenesis to obtain desired properties has constantly increasing importance (Puchkaev et al., 2002). Modifications on P450 enzymes can be done by protein design methods to improve substrate specificity, stability, solvent tolerance and activity. For these aims, heme domain is especially important. Alternative cofactors and development of electron transfer systems are also studied of improving P450 enzymes (O'Reilly et al., 2011).

Site-directed mutagenesis and directed evolution are protein design methods to create mutations on proteins. Site-directed mutagenesis was introduced by Smith and co-workers in 1970s. Site-directed mutagenesis is also referred as rational design. Point mutations are computational created by using detailed information of three-dimensional structures (Sheldon & Woodley, 2018). Rational design is promising for optimizing the desired properties for industrial applications. This approach provides understanding mechanisms of enzyme binding and catalytic mechanisms (Chen, 2001).

Directed evolution does not need information of enzyme structure. This approach employs random process such as error-prone PCR for creating mutant libraries. Genetic selection or screening determines the mutants with improved qualities (Chen, 2001). The process of directed evolution and rational design are shown in Figure 1.11.

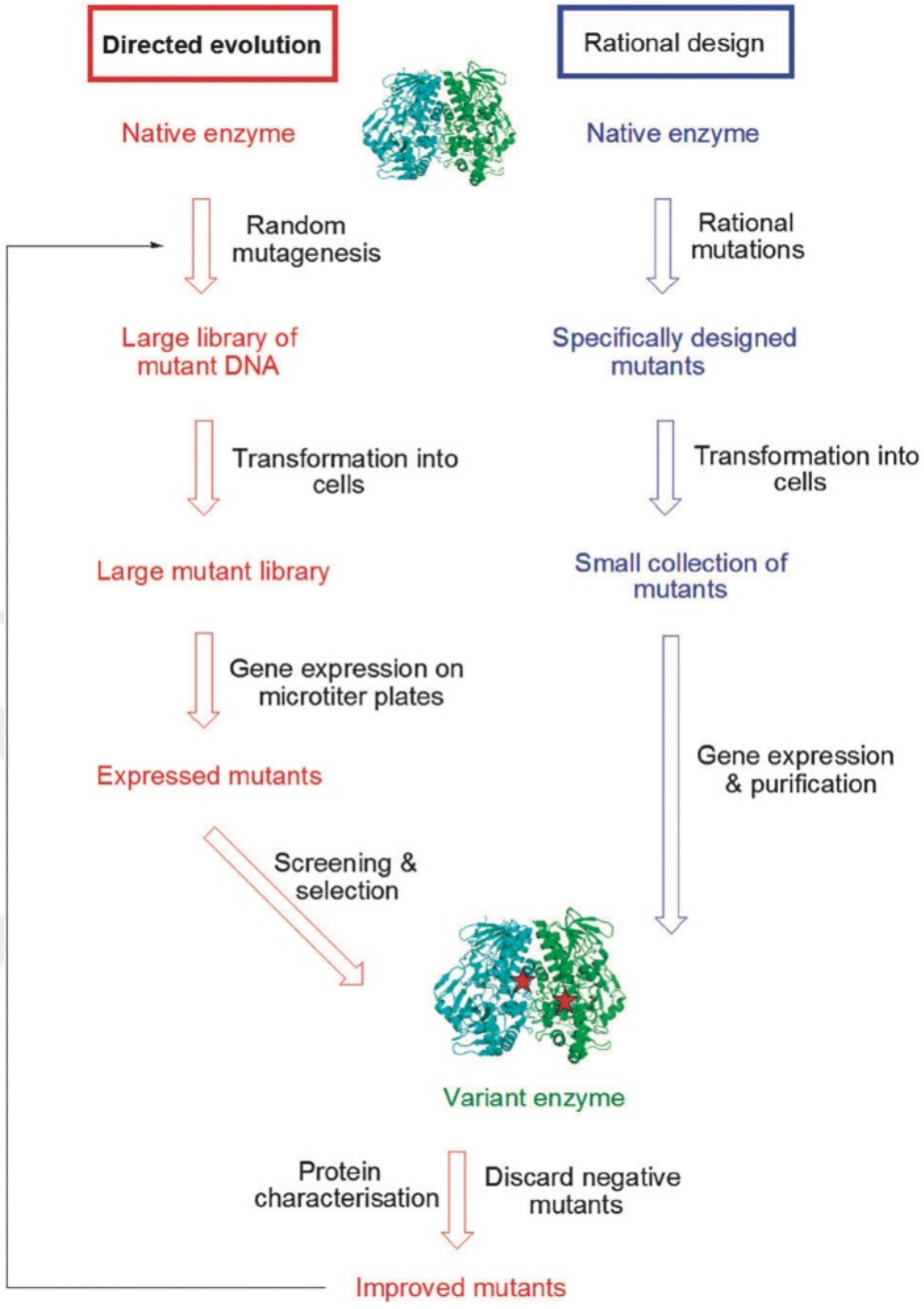

Figure 1.11. Comparison of the processes in directed evolution and rational design (O'Reilly et al., 2011).

1.6. Previous Study

Previous computational study in our laboratory aimed to use CYP119 for selective hydroxylation progesterone which is important for production of hormones like cortisone and aldosterone. In this study, other CYP enzymes which can naturally catalyze hydroxylation of progesterone were used to select residues to be mutated on CYP119 (PDB ID: 1F4T). To determine residues that cause steric hindrance with substrate, progesterone-docking was carried out. In conclusion, twelve residues containing Leu69, Val151, Phe153, Leu155, Leu205, Ile208, Ala209, Thr213, Thr214, Val254, Thr257 and Leu354 were mutated to Gly, Glu, Phe, Met, Ala, His, Arg and Ile by using DockMCM Protocol of PyRosetta program. Two coordinates of progesterone were used (Figure 1.12). Docking results were eliminated according to their energy scores. Double and triple mutants were modeled for docking studies. Elimination of double and triple mutant enzymes was carried out by energy scores (Kestevur Doğru, 2019).

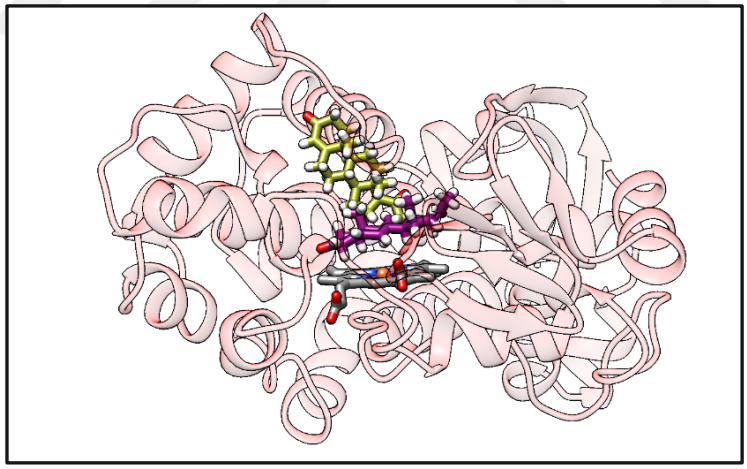

Figure 1.12. Presentation of PRG-1 (yellow) and PRG-2 (purple) in the active site of wild type CYP119 (Kestevur Doğru, 2019).

Finally, five mutants were finally selected for laboratory production. For PRG-1 docking group, T214M-I208R-F153A and L69G-L205E mutants were selected. For

PRG-2 docking group, L69G (Figure 1.13), L69G-L205G and L69G-V151A-L205G mutants were selected (Table 1.1) (Kestevur Doğru, 2019).

Hydroxylated progesterone derivatives that were predicted to be obtained by selected mutants were 1-hydroxyprogesterone, 2-hydroxyprogesterone, 11-hydroxyprogesterone and 12-hydroxyprogesterone (Kestevur Doğru, 2019).

Table 1.1. Summary of selected mutants for production in laboratory (Kestevur Doğru, 2019).

	Mutant Name	REU Score	Possible Hydroxylation Site
	WT	-567	-
PRG-1	L69G-L205E	-1183	C11
	T214M-I208R-F153A	-1210	C2
PRG-2	L69G	-1194	C12
	L69G-L205G	-1198	C1
	L69G-V151A-L205G	-1184	C1

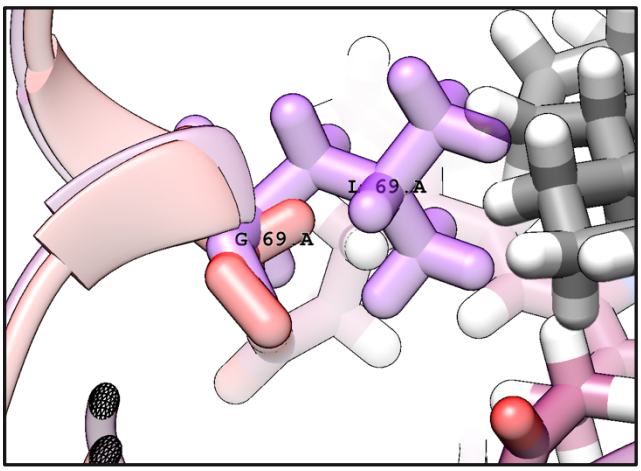

Figure 1.13. Presentation of wild type structure (purple), Gly69 mutation (red) and progesterone (grey) (Kestevur Doğru, 2019).

1.7. Scope of This Study

Previous computational study by Ekin KESTEVUR DOĞRU in our laboratory, has identified L69G mutant of the thermophilic cytochrome P450 CYP119 as a possible candidate to catalyze hydroxylated progesterone derivatives by in silico mutagenesis and docking simulations (Kestevur Doğru, 2019). This study aims to express, isolate and characterize L69G CYP119 and compare its catalytic properties with WT CYP119. To this end the L69G CYP119 was cloned by site-directed mutagenesis. WT and L69G CYP119 were expressed in *Escherichia coli*, isolation and purification of these enzymes were also performed. Amplex Red® oxidation activity of L69G CYP119 was demonstrated to be similar to WT CYP119. Catalytic effects of L69G mutation on WT CYP119 was investigated. Anew product, thought to be hydroxylated progesterone was observed as result of conversion of progesterone by L69G CYP119 using the peroxide shunt pathway in the catalytic cycle of the P450 and the same reaction was performed with WT CYP119 for comparison.

CHAPTER 2

MATERIALS AND METHODS

2.1. Materials

- The pET11a with Wild Type (WT) CYP119, primers, competent cells, kits, mediums, chemicals, and equipment used during this study are listed below.

2.1.1. The pET11a with WT CYP119 and Primers

- The pET11a with WT CYP119 was a gift from Teruyuki Nagamune (Addgene plasmid #66131) (Suzuki et al., 2014).
- The designed primers for mutation were purchased from Sentebiolab Biyoteknoloji.

2.1.2. Competent Cells, Kits and Mediums

- *Escherichia coli* (*E. coli*) DH5α competent cells were used to maximize transformation efficiency. *E. coli* BL21(DE3) competent cells were used to maximize expression efficiency.
- Q5 Site-Directed Mutagenesis Kit, Macherey-Nagel Plasmid DNA purification kit were used.
- Lysogeny Broth (LB) medium (10 g/L tryptone, 5 g/L yeast extract and 10 g/L NaCl) was used for cell growth in small scale.

- LB Agar
- 2xYT medium (16 g/L tryptone, 10 g/L yeast extract and 5 g/L NaCl at pH 6.8) was used for cell growth in large scale.
- Super Optimal Broth (SOB) medium (20 g of tryptone, 5 g of yeast extract, 0.5 g of NaCI, 10 mL of a 250 mM solution of KCl, 5 mL of a sterile solution of 2 M $MgCl_2$ per liter at pH 7.0) was used for preparation of competent cells.
- SOC medium (20 g of tryptone, 5 g of yeast extract, 0.5 g of NaCI, 10 mL of a 250 mM solution of KCl, 5 mL of a sterile solution of 2 M MgCl2, 20 mL of a sterile 1 M solution of glucose; per liter at pH 7.0) was used for transformation step.

2.1.3. Chemicals

- Ampicillin, DNA ladder, Isopropyl β-D-1-thiogalactopyranoside (IPTG), Protein Ladder
- Amplex red®, Styrene and Progesterone were used as substrates for activity assays.
- Hydrogen peroxide (H_2O_2), *tert*-butyl hydroperoxide (TBHP) and cumene hydroperoxide were used as oxidants for activity assays.

2.1.4. Equipments

- Centrifuge, Dry-Bath, pH meter, incubator, shaking incubator, Vortex, UV-Visible spectrophotometers, Water-Bath, high performance liquid chromotography (HPLC) (Agillent 1200 series and Thermo Scientific Ultimate 3000) were used during this study.

2.2. Methods

Designed L69G mutant gene was cloned. WT and L69G CYP119 were expressed, isolated and purified. Activity assays and binding studies of these enzymes were carried out.

2.2.1. Cloning of Mutant Gene by PCR

The plasmid containing WT CYP119 was a gift from Teruyuki Nagamune (Addgene plasmid #66131) (Suzuki et al., 2014). Q5 Site-Directed Mutagenesis Kit (New England BioLabs Inc., E0554S) was used for creation of designed mutant gene. The forward and reverse primers (Table 2.) were designed for desired mutation (L69G) (from CTG to GGC) and synthesized by Sentebiolab Biyoteknoloji (Ankara, Turkey). pET11a + WT CYP119 plasmid was used as template. The kit protocol was followed. The reaction was performed in 25 µL volume for PCR. Ingredients in the reaction and conditions of PCR are given Table 2.2 and Table 2.3, respectively.

Table 2.1. Primers designed to clone CYP119 with L69G mutation.

Mutation	**Primers**	
L69G	Forward:	5’ GTATACCATGGGCACCTCAGATCCC 3’
	Reverse:	5’ CTAGTGGGGATGTCGAAC 3’

Table 2.2. Reagents used in 25 µL reaction for L69G mutation by PCR.

Ingradients	Reaction	Final Concentration
Q5 Hot Start High-Fidelity 2X Master Mix	12.5 µL	1X
10 µM Forward Primer	1.25 µL	0.5 µM
10 µM Reverse Primer	1.25 µL	0.5 µM
Template DNA (1-25 ng/ µl)	1 µL	1-25 ng
Nuclease-free water	9 µL	

Table 2.3. PCR conditions.

STEP		Temperature	Time
Initial Denaturation		98 ˚C	45 sec
28 Cycles	**Denaturation**	98 ˚C	10 sec
	Annealing	58 ˚C	30 sec
	Extension	72 ˚C	3 min 22 sec
Final Extension		72 ˚C	2 min
Hold		4 ˚C	∞

PCR products were confirmed by 1% Agarose gel electrophoresis. PCR product was treated with Kinase-Ligase DpnI (KLD) enzyme mix (New England BioLabs, M05554S) for 30 mins at room temperature for removal of template plasmid and circularization of newly amplified plasmid. KLD enzyme mix allows phosphorylation by kinase, intermolecular ligation/circularization of PCR product by ligase and degradation of template DNA by DpnI. The reaction of KLD treatment was performed in 10 µL volume (Table 2.4).

Table 2.4. KLD reaction.

	10 µL Reaction	**Final Concentration**
PCR Product	1 µL	
2X KLD Reaction Buffer	5 µL	1X
10X KLD Enzyme Mix	1 µL	1X
Nuclease-free Water	3 µL	

2.2.2. Agarose Gel Electrophoresis

Agarose gel electrophoresis (1%) was carried out for confirmation of PCR products. 50X TAE buffer prepared. 50X TAE buffer includes 2 M Tris base (VWR 201-064-4), 50 mM ethylenediaminetetraacetic acid (EDTA, Bioshop Canada Inc. EDT001.1) and 1 M acetic acid (Sigma Aldrich, 27225) which were dissolved in distilled and deionized water (ddH_2O). 50X TAE buffer was diluted to 1X TAE buffer. Agarose (0.3 g) was completely dissolved in 30 mL of 1X TAE buffer in the microwave. 3 µL of 10,000X SYBP Safe DNA Gel Stain (Thermo Fisher Scientific, S33102) was added to the agarose solution when the agarose solution cooled down. After mixing, mini comb was placed to gel tray and the solution was poured into gel tray. DNA sample was prepared after the gel solution was solidified. 1X TAE buffer was filled into tank (Cleaver Scientific Ltd., MSMINIDUO). DNA sample was mixed with 6X Gel Loading Dye Purple (New England BioLabs, B7024S). 1 kb DNA ladder (New England BioLabs, N3232S) was used as ladder. DNA sample and DNA ladder were loaded into wells. The gel was run at 110 V (Bio-Rad, PowerPac Basic) until the dye line was reaches to the end of the agarose gel. Cleaver Safeview-Mini2 was used to visualize DNA sample on the gel.

2.2.3. Competent *E. coli* BL21(DE3) Cells

E. coli BL21(DE3) competent cells were streaked on LB agar plate without ampicillin and incubated overnight at 37 °C. A single colony from plate was inoculated into 25 mL LB medium and grown for 8 h at 37 °C, 220 RPM. Starter cultures (100 µL and 250 µL) were inoculated into 2 flasks of 250 mL SOB medium. The cultures were grown overnight at 18 °C, 220 RPM. In the following morning, the cultures were grown to OD_{600}=0.55 at 18 °C, 220 RPM. The flask was incubated for 10 min on ice after OD_{600} was reached 0.55. The culture (50 mL) was harvested by centrifuge at 3200 RPM for 15 min at 8 °C. The medium was discarded, and the cells were resuspended with 16 mL of Inoue Transformation buffer (55 mM manganese (II) chloride tetrahydrate ($MnCl_2 \cdot 4H_2O$), 15 mM calcium chloride dihydrate ($CaCl_2 \cdot 2H_2O$), 250 mM potassium chloride (KCl) and 0.5 M piperazine-1,2-bis (2-ethanesulfonic acid) (PIPES) pH 6.7 in ddH_2O) which was filtered and cold. The cells were harvested by centrifuge at 3200 RPM for 15 min at 8 °C. The buffer was discarded, and the cells were resuspended with 4 mL of Inoue Transformation buffer. Dimethyl sulfoxide (DMSO, 300 µL) was added and the cells in the buffer were incubated on ice for 10 mins. The cell suspension (50 µL) was transferred into each microcentrifuge tubes which were sterilized and cooled. The tubes were placed immediately into liquid nitrogen and the frozen competent cell aliquots were transferred to -80 °C.

2.2.4. Transformation and Confirmation of L69G CYP119

Plasmids with L69G mutation were transformed in *E. coli* DH5α competent cells by heat-shock transformation to maximize efficiency. For transformation method, Q5 Site-Directed Mutagenesis Kit Protocol was modified. The tube was incubated on ice. The competent cells (50 µL) were transferred to the tube. KLD reaction mixture from the PCR reaction (5 µL) was added to the cells. The cells were incubated on ice for 30 min. After 30 min, the cells were incubated at 42 °C for 45 sec for heat shock and incubated on ice for 2 min. SOC medium (950 µL) was added to the cells and incubation of the cells

was carried out by shaking at 37 °C, 220 RPM for 1 h. The cells (200 µL) were spread to LB agar plate with 0.1 g/L ampicillin and the remaining cells were pelleted at 3800 RPM for 10 min. The medium (800 µL) was removed and cell pellet was resuspended with the remaining medium. Resuspended cells were spread to LB agar plate with 0.1 g/L ampicillin.

The plasmids from *E. coli* DH5α competent cells were isolated and sequenced for confirmation of desired mutation. For plasmid isolation, a single colony selected from the plate was inoculated to 7 mL LB medium with 0.1 g/L ampicillin and grown overnight at 37 ºC, 220 PRM. The protocol of Macherey-Nagel Plasmid DNA purification kit was followed for the isolation. The cells were harvested by centrifugation at 3800 RPM for 15 min. The cell pellets were resuspended by adding 250 µL of Buffer A1 by pipetting up and down and then transferred to 1.5 mL eppendorf tube. Buffer A2 (250 µL) was added to the tube and the tube was inverted gently 6-8 times and the incubation was performed at room temperature for 5 min. Buffer A3 (300 µL) was added to the tube and the tube was inverted gently 6-8 times until blue samples turn colorless during cell lysis step. For clarification of lysate, centrifugation was performed at 11,000 g for 5 min at room temperature. To bind DNA, NucleoSpin® Plasmid column was placed in the collection tube and the supernatant was decanted onto the column. Centrifugation was performed at 11,000 g for 1 min. Flow through was discarded and column was placed in the collection tube again. To wash silica membrane, 600 µL Buffer A4 was added and the tube was centrifuged at 11,000 g for 1 min. Flow through was discarded. Column was placed in collection tube again and the tube was centrifuged at 11,000 g for 2 min to dry silica membrane. To elute DNA, the column was placed in the new collection tube and 50 µL of Buffer AE was added onto column. Plasmid DNA was collected to 1.5 mL eppendorf tubes by centrifugation at 11,000 g for 1 min.

Concentrations of eluted plasmids were calculated by measuring with Thermo Fisher Scientific Multiskan GO (1068879) and µDrop Plate (Thermo Scientific, N12391). Concentration of plasmids was arranged to desired concentration for sequencing. Sequencing of plasmids was done by Triogen Biotech. Result of sequence was checked by Geneious Prime.

The confirmed plasmids were transformed in *E. coli* BL21(DE3) competent cells by heat-shock transformation to maximize expression efficiency. The same steps for transformation of plasmids to *E. coli* DH5α competent cells was performed. A single colony which was selected from plate was inoculated to LB medium. The cells grown

overnight at 37 °C, 220 RPM by shaking. In following morning, glycerol stock of the cells was prepared by transferring 1:1 glycerol/the cells solution in medium to cryogenic tubes and stored at -80 °C.

2.2.5. Expression of Recombinant WT and L69G Mutant CYP119

E. coli BL21(DE3) competent cells, containing plasmids with WT CYP119 and L69G mutation, from glycerol stocks were cultured overnight in 10 mL LB medium with 0.1 g/L ampicillin at 37 °C and 220 RPM. The cells (1% of medium volume) were inoculated to 2xYT Medium with 0.1 g/L ampicillin and grown at 37 °C and 220 RPM. The cells were incubated until OD600 reached ~0,8 at 37 °C and 220 RPM. Protein expression in *E. coli* BL21(DE3) competent cells were induced using 1 mM isopropyl-1-thio- β-D-galactopyranoside (IPTG). The cells were incubated at 30 °C, 220 RPM for 30 h by shaking. The cells were harvested at 3200 rpm for 45 min at 25 °C. Pellets were stored at -80 °C for least one night.

2.2.6. Isolation and Purification of Recombinant WT and L69G Mutant CYP119

The frozen cell pellets, which stored at -80 °C, were resuspended with lysis buffer (Table 2.5). The cells were sonicated for 30 secs with 1 min interval five times and then the cell lysate was incubated in water bath 65 °C for 1 h. Centrifugation was performed at 3900 RPM at 4 °C for 1.5 h to remove the cell debris. WT CYP119 and L69G CYP119 enzymes were isolated from supernatant by discarding the cell pellet. First, the supernatant was exposed to 40% ammonium sulphate and proteins were removed by centrifugation at 3900 RPM for 45 min at 4 °C. The supernatant was subjected to 60% ammonium sulfate. Centrifugation was carried out at 3900 RPM at 4 °C for 1.5 h. The supernatant was then removed and the precipitate was resuspended with dialysis buffer (Table 2.5) and dialyzed against the same buffer to remove ammonium sulphate by using

dialysis membrane (10-14 K MWCO). Purity of the enzymes was analyzed with SDS-PAGE and heme incorporation was analyzed by ratio of Abs415/Abs280 by using UV-Visible spectra. Enzymes were concentrated by concentrator (with 10 K MWCO). The concentrated enzymes (50 µL) were transferred into each microcentrifuge tubes and stored at -80 °C.

Table 2.5. The buffers for isolation and purification of WT and L69G CYP119.

Ingradients	Lysis Buffer	Dialysis Buffer
0.1 M Potassium Phosphate Buffer	50 mM	50 mM
NaCl	150 mM	20 mM
Benzamidine HCl	1 mM	-
Phenylmethylsulfonyl Fluoride (PMSF)	0.2 mM	-
Glycerol	-	5%
	in dH_2O	in ddH_2O
pH	7.5	7.4

2.2.7. Sodium Dodecyl Sulfate Polyacrylamide Gel Electrophoresis (SDS-PAGE) Analysis of WT and L69G Mutant CYP119

Confirmation of L69G CYP119 protein band was confirmed by Sodium Dodecyl Sulfate Polyacrylamide Gel Electrophoresis (SDS-PAGE) (15%). Molecular weight of L69G mutant is 43 kDa. Protein bands were monitored for steps of expression, isolation and purification of WT and L69G CYP119 by SDS-PAGE. Purity of the enzymes was analyzed.

2.2.8. UV-Vis Spectroscopic Analysis of WT and L69G Mutant CYP119

UV-Visible spectra of WT and L69G CYP119 in 50 mM potassium phosphate buffer at pH 7.4 was analyzed in 250-650 nm by using VWR® UV/1600PC Scanning Spectrophotometer. Concentrations of the enzymes was calculated by using the extinction coefficient of CYP119 (ε_{415nm} = 104 $mM^{-1} \cdot cm^{-1}$) and absorbance in 415 nm in Equation 2.1.

$$A = C \cdot \varepsilon \cdot L \tag{2.1}$$

A: Absorbance
C: The concentration of the sample
Ɛ: Specific-extinction coefficient
L: The optical path length

2.2.9. Substrate Binding Assays by WT and L69G Mutant CYP119

Lauric acid and progesterone were used as substrates for ligand binding assays of the enzymes. Binding constants for substrates were determined at room temperature by difference spectroscopy using VWR® UV/1600PC Scanning Spectrophotometer. K_S values were calculated by using quadratic equation (Equation 2.2) and compared with each other (Koo et al., 2002).

$$\Delta A = \frac{A_{max}}{[E]}\left(\frac{K_S+[E]+[L]-\sqrt{(K_S+[E]+[L])^2-4[E][L]}}{2}\right) \tag{2.2}$$

2.2.9.1 Lauric Acid Titration

Lauric acid titration was performed by following change in UV-Visible spectra in the increasing concentration of substrate. Enzyme (1.5 μM) solutions were prepared in 50 mM potassium phosphate buffer at pH 7.4 and incubated at room temperature for 10 min. The enzyme solutions were divided to two glass cuvettes. Stock solution of lauric acid was prepared in a dimethyl sulfoxide (DMSO). Lauric acid was titrated into the sample cuvette containing the enzyme solution. The amount of DMSO in the cuvette did not exceed 1% of the initial volume. Equal volume of DMSO was added to the reference cuvette. K_S value was calculated by plotting the absorbance shift between 386 and 418 nm against substrate concentration and compared each other.

2.2.9.2 Progesterone Titration

The substrate binding was followed by difference spectra using UV-1600PC Scanning Spectrophotometer. Two glass cuvettes were used. The binding assay was carried out in 2100 μL. The enzyme solutions (1.5 μM) were prepared in 50 mM potassium phosphate buffer at pH 7.4 and kept for 10 min at room temperature. The cuvettes were contained the enzyme solutions. Progesterone as substrate was dissolved in DMSO at stock concentration of 7 mM. The enzyme solutions were divided to two cuvettes. Two cuvettes were used as reference cuvette and sample cuvette. One of the cuvettes was titrated with increasing substrate concentration while the other cuvette was titrated with the same amount of DMSO. The absorbance shifts between 394 nm and 426 nm for progesterone titration of WT CYP119 and 390 nm and 420 nm for progesterone titration of L69G CYP119 were followed. The absorbance shift was plotted against to concentration of progesterone. K_S value for progesterone was calculated by using Equation 2.2 and compared each other.

2.2.10. Activity Assays by WT and L69G Mutant CYP119

Some artificial substrates containing Amplex Red® and styrene were catalyzed by CYP119. So, peroxidase activity with Amplex Red® and styrene epoxidation were performed for activity assays of WT and L69G CYP119 and compared with each other. Natural substrates of CYP119 have not been found, yet. Cytochrome P450 monooxygenases can play role in steroid hydroxylation. Progesterone hydroxylation was carried out with L69G CYP119 which was important contact with progesterone as predicted in the previous study. Conversion of progesterone with L69G CYP119 was compared to conversion of progesterone with WT CYP119.

2.2.10.1 Amplex Red® Peroxidation

Amplex Red® peroxidation reactions were optimized by performing reactions without enzyme. The reactions contained 10 µM Amplex Red® and 1.5 mM H_2O_2 in 50 mM potassium phosphate buffer at pH 7.4. Also, the reactions were performed by addition of 1 mM EDTA to prevent metal ions in the buffer. Formation of the product (Resorufin) was followed with absorbance changes in 570 nm by the time (0, 5, 10, 20, 30, 45, 60, 90, 120, 150, 180 min).

Amplex Red® peroxidation was set up with 10 µM Amplex Red®, 1.5 µM enzyme, 1.5 mM H_2O_2 and 1 mM EDTA in 50 mM potassium phosphate buffer at pH 7.4 at room temperature for enzyme activity assays. Absorbance changes in 570 nm were followed by the time (0, 2, 5, 10, 20, 30, 45, 60 min) because resorufin formed as result of the reaction (Figure 2.1) give a pink color.

Different concentrations of H_2O_2 were used in the reactions for the kinetic analysis by the same reaction conditions. Kinetic parameters (k_{cat}, K_m and V_{max}) were determined by nonlinear fitting using Michealis-Menten. L69G CYP119 was compared with WT CYP119.

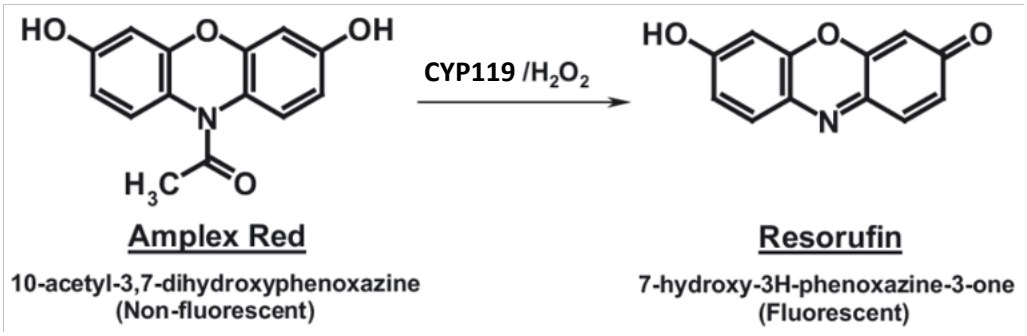

Figure 2.1. Amplex Red oxidation into Resorufin catalyzed by CYP119 using H_2O_2.

2.2.10.2 Styrene Epoxidation

Styrene epoxidation was catalyzed by CYP119 by using *tert*-buthyl hydroperoxide (TBHP) as oxidants. Styrene oxide forms as result of styrene epoxidation (Figure 2.2). Conditions for styrene epoxidation was performed by following the studies of Zhang et al. (Zhang et al., 2014) with some modifications. Each 100 µL reaction was contained 3.5-7 mM styrene, 12.5 µM enzyme and 7 mM TBHP in 50 mM potassium phosphate buffer at pH 7.4 for 15, 30, 60, 90 min. The reactions were performed in the closed glass vials at room temperature. The reactions were quenched with 900 µL acetonitrile and filtered by 0.45 µm polytetrafluoroethylene (PTFE) filters into the new glass vials. Analysis of the reactions was performed with high performance liquid chromatography (HPLC) on Thermo Scientific Ultimate 3000 coupled with UV detector fixed 220 nm. Nucleodur C18 column (Macherey-Nagel) (25 × 0.46 cm, 5 µm) was used for analysis on HPLC. Mobile phase of HPLC was 30 : 70 ddH_2O : acetonitrile. Different concentrations of styrene solutions and styrene oxide 98+% in acetonitrile was prepared to form standard calibration curves. The concentration of styrene oxide formed from the reactions was calculated by using linear equation of calibration curve. The retention times were determined as 6.5 min for styrene and 4.27 min for styrene oxide. The reactions were carried out for variable concentration of styrene (3.5-7 mM) with constant concentration of oxidant for 10 min. Kinetic parameters (k_{cat}, K_m and V_{max}) were determined by nonlinear fitting using Michealis-Menten. L69G and WT CYP119 were compared each other.

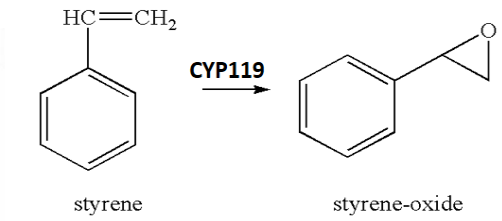

Figure 2.2. Styrene epoxidation by CYP119.

2.2.10.3 Conversion of Progesterone

The conversion of progesterone was carried out in 250 µL reaction containing 10 µM WT and L69G CYP119 and 150 µM progesterone in 50 mM potassium phosphate buffer at pH 7.4. After incubation for 5 min at room temperature, the reaction was started by adding an oxidant. Cumene hydroperoxide (1 and 5 mM), *tert*-buthyl hydroperoxide (TBHP, 3 and 7 mM) and hydrogen peroxide (H_2O_2, 1 and 10 mM) were used as oxidants. The reaction was continued for 30 min and quenched by adding 250 µL ethyl acetate. The negative control was the same reaction without enzyme. The conversion of progesterone was confirmed by thin layer chromatography (TLC). Solvent system for analysis was 97 : 3 $CHCl_3$: MeOH.

For kinetic analysis, the reactions were consisted of 10 µM enzyme and 0-150 µM progesterone in 50 mM potassium phosphate buffer at pH 7.4 in total volume of 500 µL. The reaction was carried out at room temperature. Enzyme and substrate in the buffer were incubated for 5 min before the reaction. The reaction was initiated by addition of 1 mM cumene hydroperoxide and performed for 30 min and stopped by addition 500 µL ethyl acetate. The reaction was extracted thrice with 1:1 ethyl acetate and ethyl acetate was evaporated by nitrogen gas. The residues were dissolved in 1 mL methanol and analyzed to high performance liquid chromatography (HPLC).

The HPLC analysis was performed on Agilent 1200 Series by DAD detector. Teknokroma Mediterranea Sea18 RP-C18 (15 × 0.46 cm, 5 µm) column was used for experiments. Reactions were analyzed by HPLC. The HPLC run started with 40:60 acetonitrile: ddH_2O for 4 min, increasing 100:0 acetonitrile: ddH_2O for 11 min and 40:60 acetonitrile: ddH_2O for 5 min at flow rate of 1 mL/min. Detection of substrate, oxidant and products was accomplished at 225 nm and 254 nm

2.2.11. Reactions of WT and L69G Mutant CYP119 with Peroxides

Hydrogen peroxide, *tert*-buthyl hydroperoxide and cumene hydroperoxide were used respectively for Amplex Red® oxidation, styrene epoxidation and hydroxylation of progesterone by WT and L69G CYP119. Thus, degradation of heme was investigated by the reaction of the enzymes with peroxides. The chemical structures of peroxides used in this thesis are shown in Figure 2.3.

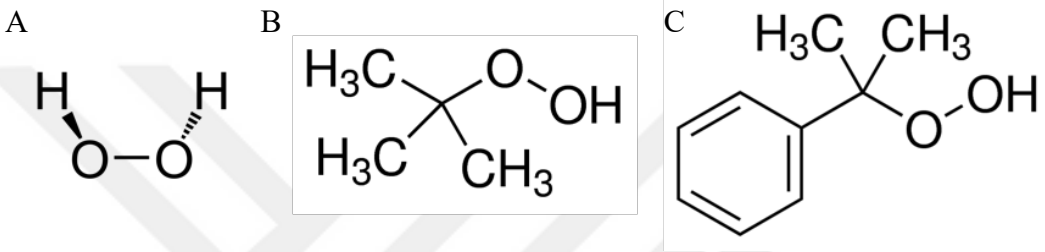

Figure 2.3. Peroxides were used for reactions. Hydrogen peroxide (H_2O_2) (A). *tert*-buthyl hydroperoxide (TBHP) (B). Cumene hydroperoxide (C).

2.2.11.1 Reaction of WT and L69G Mutant CYP119 with Hydrogen Peroxide

Reactions with hydrogen peroxide (H_2O_2) reactions were carried out with WT and L69G CYP119. The Soret absorbance of CYP119 at 414 nm was followed. Reactions contained 1 mM EDTA, 1.5 µM enzyme and 1.5 mM H_2O_2 in 50 mM potassium phosphate buffer at pH 7.4. After H_2O_2 was added to the reaction, UV-Visible spectra were taken at 0, 2, 5, 10, 20, 30 and 45 min.

2.2.11.2 Reaction of WT and L69G Mutant CYP119 with *tert*-Buthyl hydroperoxide

Reactions of WT and L69G CYP119 with *tert*-buthyl hydroperoxide (TBHP) were analyzed. For heme degradation, the Soret absorbance of CYP119 at 414 nm was followed. Reactions involved 1.5 μM enzyme and 7 mM TBHP in 50 mM potassium phosphate buffer at pH 7.4. Following addition of TBHP in the reaction, UV-Visible spectra were taken at 0, 2, 5, 10, 20, 30, 45, 60, 90 and 120 min.

2.2.11.3 Reaction of WT and L69G Mutant CYP119 with Cumene Hydroperoxide

Reactions of WT and L69G CYP119 with cumene hydroperoxide were analyzed. The Soret absorbance of CYP119 at 414 nm was followed to monitor heme degradation during the reaction. Reactions included 1.5 μM enzyme and 1 mM cumene hydroperoxide in 50 mM potassium phosphate buffer at pH 7.4. UV-Visible spectra were taken at 0, 2, 5, 10, 20, 30, 45, 60, 90, 120 and 150 min after addition of cumene hydroperoxide.

CHAPTER 3

RESULTS AND DISCUSSION

3.1. Cloning of L69G Mutant CYP119 by Polymerase Chain Reaction

Computational design of CYP119 for increased progesterone activity predicted increased activity for L69G CYP119 (Kestevur Doğru, 2019). L69G CYP119 is expected to bind and convert progesterone to hydroxylated progesterone by oxidation. The DNA CYP119 in pET11a was a gift from Teruyuki Nagamune (Addgene library #66131) (Suzuki et al., 2014). Forward and reverse primers (shown in Materials and Methods section) were designed for L69G mutation at WT CYP119 gene. PCR product with these primers was confirmed on 1% agarose gel. Length of CYP119 + pET11a is 6748 bp. 1% Agarose gel of PCR product is demonstrated in Figure 3.1; 1 kb DNA ladder was used in the agarose gel.

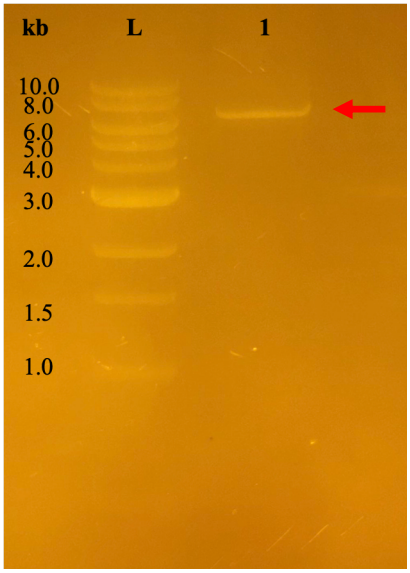

Figure 3.1. PCR products of L69G mutation of CYP119 in pET11a in 1% agarose gel. L: Molecular weight standard; 1. L69G CYP119 in pET11a.

3.2. Transformation and Confirmation of L69G mutant of CYP119

PCR products initially were transformed to *E. coli* DH5α competent cells. After transformation, colonies with mutant plasmids were obtained in LB agar plates with ampicillin (Figure 3.2). Plasmids were isolated from selected two colonies. Plasmids molecular weight were confirmed by 1% agarose gel (Figure 3.3).

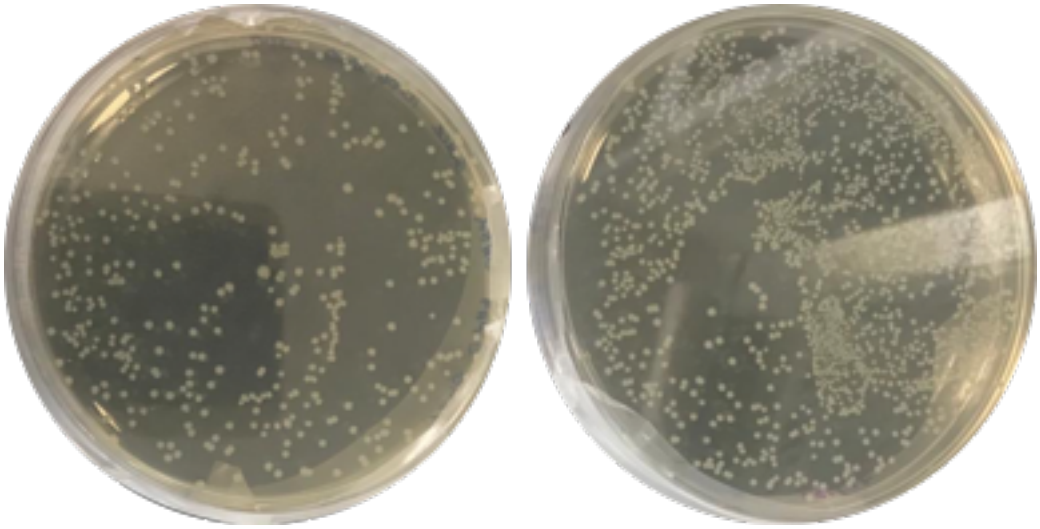

Figure 3.2. Colonies obtained in plates with ampicillin after transformation of plasmid with L69G mutation into *E. coli* DH5α competent cells.

Plasmids were sequenced by Triogen Biotech. Result of the sequence analysis by Geneious Prime software is shown in (Figure 3.3). Point mutation on WT CYP119 gene was observed. Codon of leucine (CTG) was changed codon of glycine (GGC) (Figure 3.3).

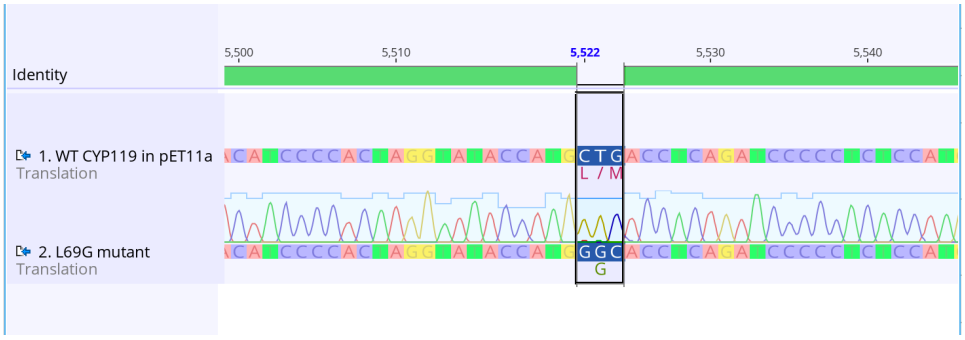

Figure 3.3. Sequence of desired mutation (L69G) on WT CYP119 gene confirmed by analysis with Geneious Prime software.

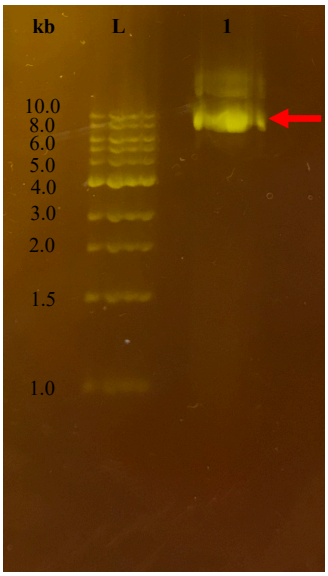

Figure 3.4. Plasmids with L69G mutation on WT CYP119 gene from *E. coli* DH5α competent cells in 1% agarose gel. L: Molecular weight standard; 1. L69G CYP119 with pET11a.

After sequence confirmation, recombinant plasmids containing L69G CYP119 were transformed into *E. coli* BL21(DE3) competent cells. A colony was selected from plate (Figure 3.5) with ampicillin (0.1 g/L) and grown overnight in LB medium with 0.1 g/L ampicillin at 37 °C, 220 RPM. The glycerol stock from the cell culture was prepared and stored at -80 °C.

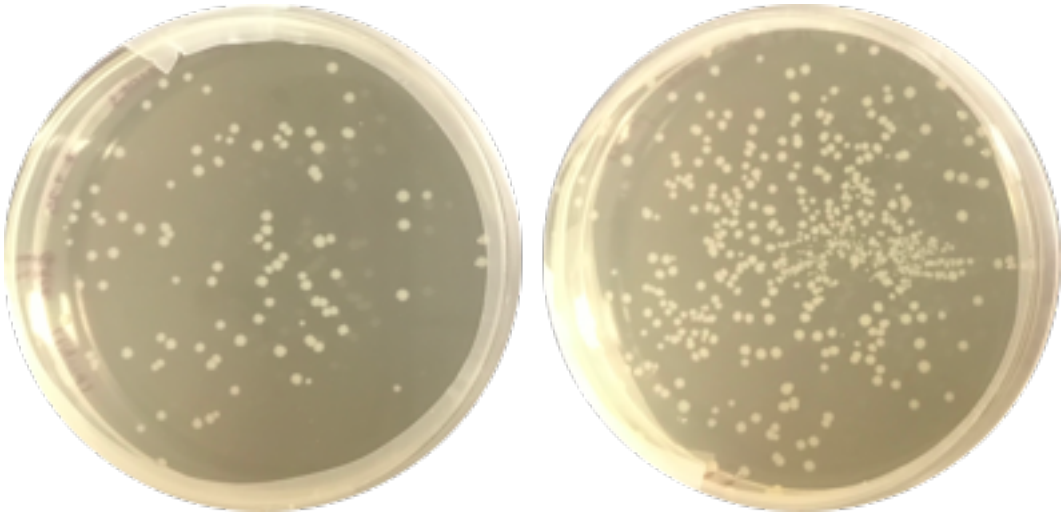

Figure 3.5. Colonies obtained in plates with ampicillin after transformation of plasmid with L69G mutation into *E. coli* BL21(DE3) competent cells.

3.3. Expression of Recombinant WT and L69G Mutant CYP119

Optimization of WT CYP119 protein expression in *E. coli* was studied by Yaprak Aslantaş (Aslantas & Surmeli, 2019; Aslantaş, 2018). Same conditions were followed for expression of L69G mutant of CYP119. The expression test for L69G CYP119 was carried out by selecting two colonies from the plate (shown in Figure 3.6). Expression of L69G CYP119 by addition of 1 mM IPTG was confirmed by 15% SDS-PAGE analysis as shown in Figure 3.6. Induction of expression by IPTG was observed by a protein band at 43 kDa (molecular weight of CYP119), as seen in Figure 3.6. After confirmation of expression, large scale production of L69G CYP119 was performed in four 500 mL flasks.

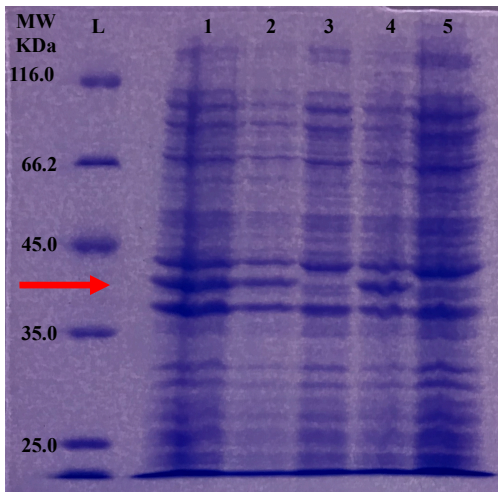

Figure 3.6. SDS-PAGE of expression of L69G CYP119 by addition of IPTG for two colonies. L: protein molecular weight marker (Thermo Scientific™ #26610). Lane 1,2: Colony 1 selected from LB agar plate after induction with IPTG for 3 h. Lane 3: Colony 1 selected from LB agar plate before addition of IPTG. Lane 4: Colony 2 selected from LB agar plate after induction with IPTG for 3 h. Lane 5: Colony 2 selected from LB agar plate before addition of IPTG (43 kDa).

3.4. Isolation and Purification of WT and L69G Mutant CYP119

After protein expression, WT and L69G CYP119 were isolated and purified as described in the Materials and Methods section. The enzymes were concentrated after purification. SDS-PAGE analysis of samples for each isolation and purification steps for WT CYP119 are shown in Figure 3.7. SDS-PAGE analysis of samples for each isolation and purification steps for L69G CYP119 are shown in Figure 3.8. The final concentrations of purified WT and L69G CYP119 were calculated 257 µM and 205 µM, respectively. From 1 L of the cell culture 11 mg of WT CYP119 was obtained. 17 mg of L69G CYP119 was obtained from 2 L of the cell culture. Purity was analyzed by SDS PAGE analysis as shown in Figure 3.9. The ratio of Abs_{415nm} and Abs_{280nm} which correlates with heme incorporation was obtained by using UV-Vis spectra. Abs_{415nm}/Abs_{280nm} was about 0.65 for both WT and L69G CYP119 after dialysis (shown in Figure 3.10). Therefore, similar levels of heme incorporation were observed for both enzymes.

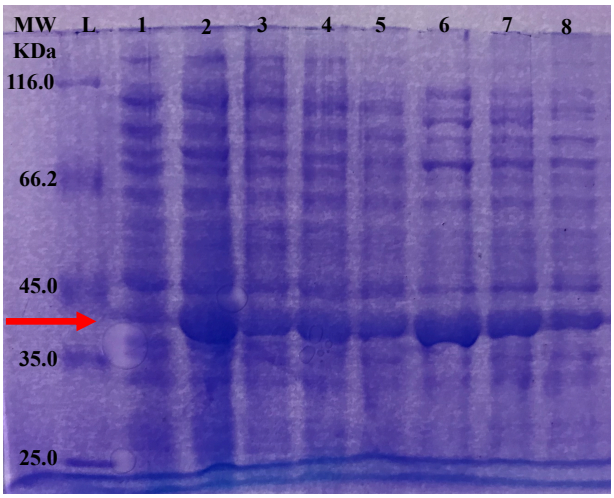

Figure 3.7. 15% SDS-PAGE analysis of the expression and isolation of WT CYP119. L: protein molecular weight marker (Thermo Scientific™ #26610). Lane 1: WT CYP119 with no IPTG. Lane 2: WT CYP119 with IPTG. Lane 3. After sonication step. Lane 4: Pellet after centrifuge following sonication step. Lane 5: Supernatant after centrifuge step following heat treatment. Lane 6: Pellet after 40% ammonium sulphate precipitation. Lane 7: Supernatant after 40% ammonium sulphate precipitation. Lane 8: 60% ammonium sulphate precipitation on supernatant (43 kDa).

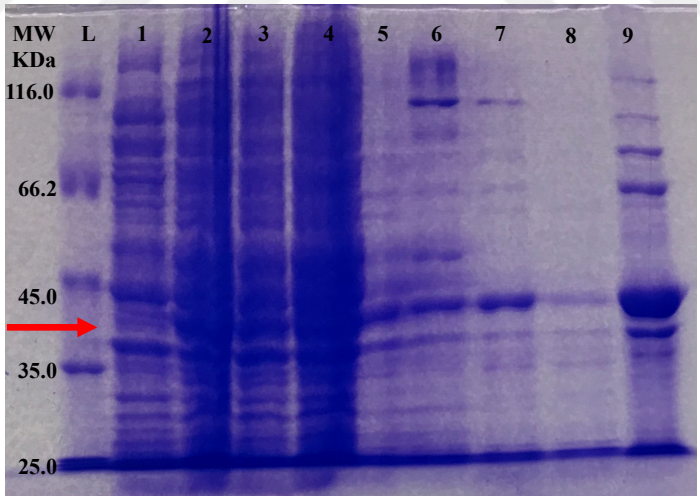

Figure 3.8. 15% SDS-PAGE analysis of the expression and isolation of L69G CYP119. L: protein molecular weight marker (Thermo Scientific™ #26610). Lane 1: L69G CYP119 with no IPTG. Lane 2: L69G CYP119 with IPTG. Lane 3. After sonication step. Lane 4: Pellet after centrifuge following sonication step. Lane 5: Supernatant after centrifuge step following heat treatment. Lane 6: Pellet after 40% ammonium sulphate precipitation. Lane 7: Supernatant after 40% ammonium suphate precipitation. Lane 8: 60% ammonium sulphate precipitation on supernatant. Lane 9: Purified L69G CYP119 (43 kDa).

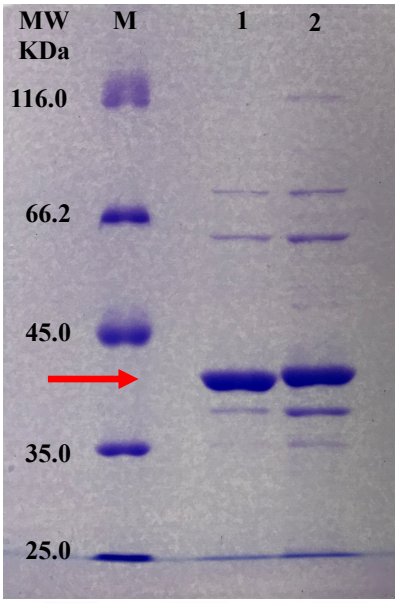

Figure 3.9. 15% SDS-PAGE analysis of L69G and WT CYP119 after purification. M: protein molecular weight marker (Thermo Scientific™ #26610). Lane 1: WT CYP119. Lane 2: L69G CYP119 (43 kDa).

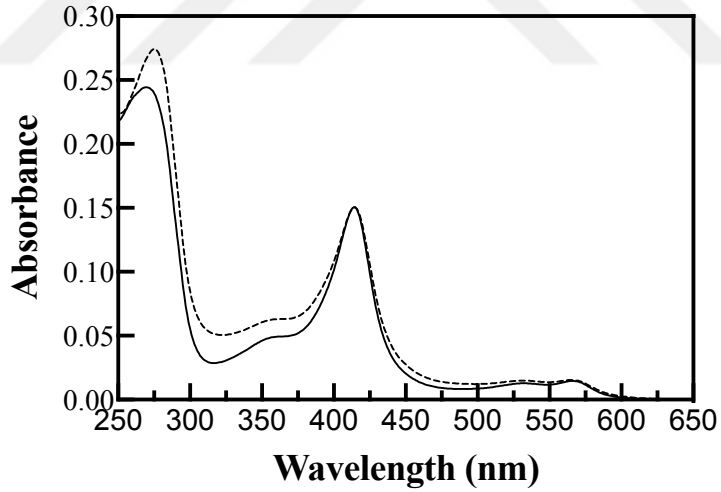

Figure 3.10. The UV-Visible spectra of WT and L69G CYP119 for analysis of heme incorporation based on Abs_{415nm}/Abs_{280nm} (Solid: WT CYP119; dash: L69G CYP119).

3.5. Spectroscopic Analysis of WT and L69G Mutant CYP119

The comparison of optical spectra of WT and L69G CYP119 are shown in Figure 3.11. For WT CYP119 maximum Soret absorbance was observed at 414 nm. WT CYP119 shows splitting of alpha-beta (α/β) bands at 531 nm and 564 nm (Aslantaş, 2018). L69G mutation did not result in a shift in the Soret maximum (414 nm). L69G mutation resulted in modest splitting of the α/β region as seen in Figure 3.11. inset.

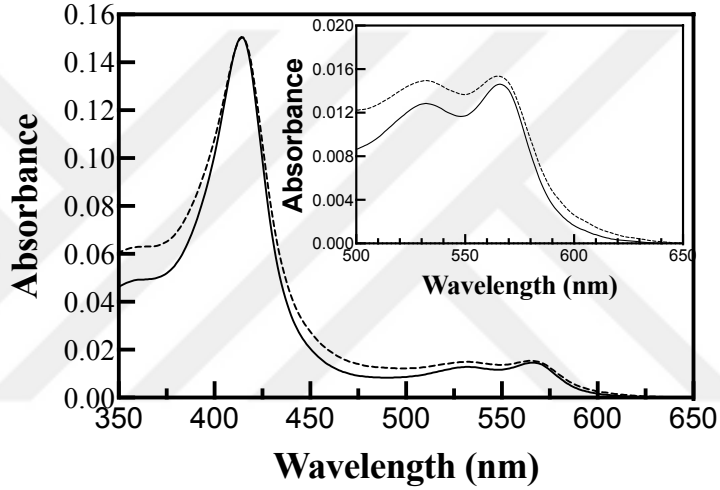

Figure 3.11. The comparison of UV-Visible spectra of WT and L69G CYP119 (Solid: WT CYP119; dash: L69G CYP119). Inset: the changes observed in the alpha-beta region.

3.6. Substrate Binding by WT and L69G Mutant CYP119

Lauric acid and progesterone were used as substrates for ligand binding studies of WT and L69G CYP119.

3.6.1. Lauric Acid Titration

The effect of the mutation on lauric acid binding to CYP119 was investigated. Binding of lauric acid to CYP119 heme active site results in a spin change of the heme iron which can be monitored through changes in Soret absorbance maximum. K_S values were calculated from the magnitude of the spin state change which is linked to the magnitude of the absorbance shift (Figure 3.12). Electronic absorption spectrum of heme depends on ligand binding (Nienhaus & Nienhaus, 2005). Conformation of the active site is changed by ligand binding. The iron in the active site alters from a low spin state to a high spin state. The spin state is the energy related to the iron and substurate. The energy change depends on difference spectra observed when the binding of enzyme and ligand is measured spectrophotometrically (Cook et al., 2016). The spectra was taken during itration with lauric acid. Difference spectra was obtained. Difference spectra of WT CYP119 was larger than difference spectra of L69G CYP119 (Figure 3.12.A and Figure 3.12.B, respectively). The absorbance shifts were observed in 386 nm and 418 nm for lauric acid titration of WT CYP119 and 384 nm and 416 nm for lauric acid titration of L69G CYP119. The absorbance difference $\Delta\Delta Abs_{(418\ nm\ -\ 386\ nm)}$ for progesterone titration of WT CYP119 and $\Delta\Delta Abs_{(416\ nm\ -\ 384\ nm)}$ for lauric acid titration of L69G CYP119 versus concentration of lauric acid was plotted (Figure 3.12.C). Using equation as described in the materials and methods section 2.2.9, K_S value of L69G was calculated as 24.3 ± 7.4 μM while K_S value of WT CYP119 was calculated as 16.8 ± 4.5 μM. L69G mutation caused decrease in the affinity to lauric acid.

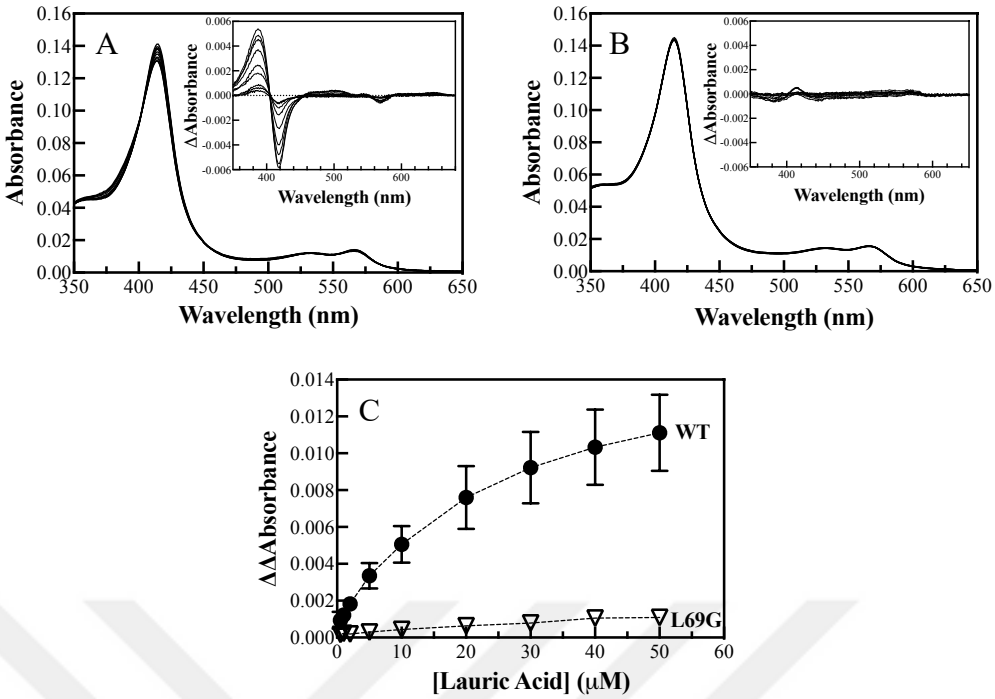

Figure 3.12. The UV–Visible and difference spectra of WT CYP119 (A) and L69G CYP119 (B) observed with titration of lauric acid. The insets show difference spectra with increasing concentrations of lauric acid (0-50 μM). The absorbance shifts observed in 386 nm and 418 nm for lauric acid titration of WT CYP119 and 384 nm and 416 nm for lauric acid titration of L69G CYP119. The absorbance difference ($\Delta\Delta Abs_{(418\ nm\ -\ 386\ nm)}$ for progesterone titration of WT CYP119 (●) and $\Delta\Delta Abs_{(416\ nm\ -\ 384\ nm)}$ for lauric acid titration of L69G CYP119 (▽)) versus concentration of lauric acid was plotted (C).

3.6.2. Progesterone Titration

The effect of the L69G mutation on progesterone binding of CYP119 was investigated. K_S values were calculated from the magnitude the spin state change which is linked to the magnitude of the absorbance shift (Figure 3.13). The absorbance shifts observed in 394 nm and 426 nm for progesterone titration of WT CYP119 and 390 nm and 420 nm for progesterone titration of L69G CYP119. The absorbance difference $\Delta\Delta Abs_{(426\ nm\ -\ 394\ nm)}$ for progesterone titration of WT CYP119 and $\Delta\Delta Abs_{(420\ nm\ -\ 390\ nm)}$ for progesterone titration of L69G CYP119 versus concentration of progesterone were plotted (Figure 3.13.C). K_S value of L69G CYP119 was calculated as 34.6 ± 7.4 μM. WT

CYP119 could not be saturated with progesterone at the maximum concentration used due to low solubility of progesterone in water. From the data in Figure 3.13.C, the K_S value was calculated to be 69.8 ± 48.9 mM for WT CYP119. These results show that L69G CYP119 has significantly higher affinity for progesterone compared to WT CYP119 as predicted by computational analysis.

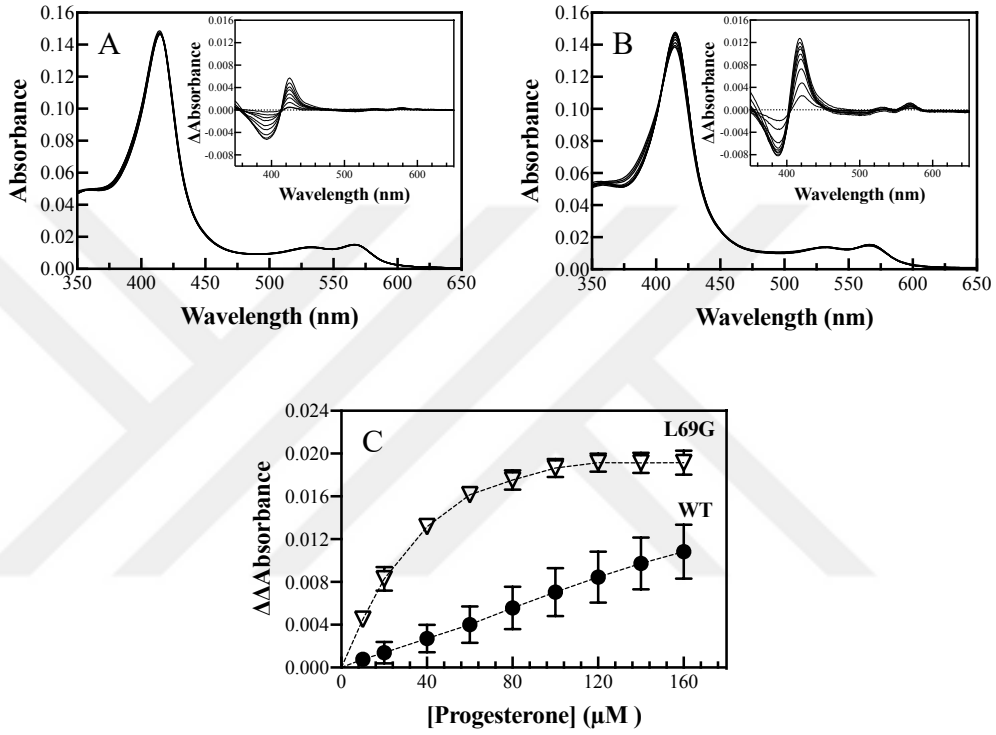

Figure 3.13. The UV–Visible and difference spectra of WT CYP119 (A) and L69G CYP119 (B) observed during the titration of progesterone. The insets show difference spectra with increasing concentrations of progesterone (0-160 μM). The absorbance shifts observed in 394 nm and 426 nm for progesterone titration of WT CYP119 and 390 nm and 420 nm for progesterone titration of L69G CYP119. The absorbance difference ($\Delta\Delta Abs_{(426\ nm\ -\ 394\ nm)}$ for progesterone titration of WT CYP119 (●) and $\Delta\Delta Abs_{(420\ nm\ -\ 390\ nm)}$ for progesterone titration of L69G CYP119 (▽)) versus concentration of progesterone (C).

3.7. Oxidation Activity of WT and L69G Mutant CYP119

Activity assays of WT and L69G CYP119 were tested by using different substrates and oxidants. Substrates used were Amplex Red®, styrene and progesterone. Hydroperoxide (H_2O_2), *tert*-buthyl hydroperoxide and cumene hydroperoxide were used as oxidant.

3.7.1. Kinetic Analysis of Amplex Red® Oxidation

Amplex Red® oxidation was firstly optimized without enzyme. Amplex Red® (10 μM) was reacted with H_2O_2 (1.5 mM) for 180 min. The product resorufin can be followed by spectroscopic analysis because resorufin gives a pink color with maximum absorbance at 570 nm. The spectra of the reaction without EDTA were shown in Figure 3.14.A. Increase in the product formation continued with time. So, the reaction was set up with addition of 1 mM EDTA. EDTA is commonly used to chelate metal ions to investigate enzyme function in the absence of metal ions. EDTA is negatively charged and optically inactive. Structure of EDTA adopts a stable conformation when complexed with a single divalent metal ion (Lopata et al., 2019). The spectra of the reaction with 1 mM EDTA were shown in Figure 3.14.B. Resorufin formation in the presence of EDTA was modest compared to EDTA free buffer (Figure 3.14.C). Addition of EDTA was important to analyze only enzyme activity.

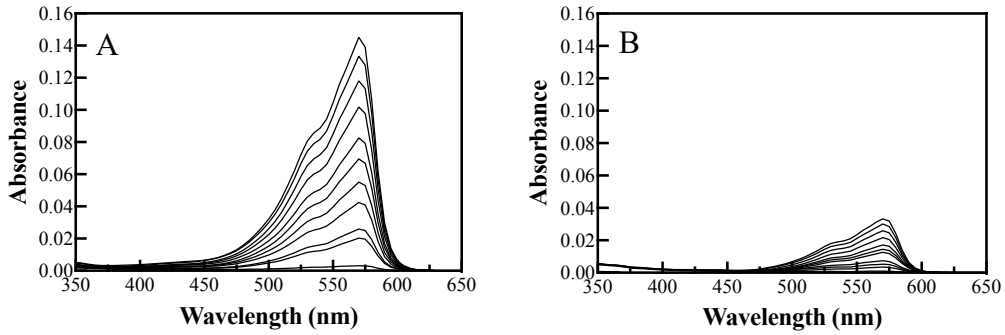

Figure 3.14. UV-Visible spectra of Amplex Red® oxidation analysis in the absence of enzyme. The spectra were taken at 0, 5, 10, 20, 30, 45, 60, 90, 120, 150 and 180 min. The reaction in 50 mM potassium phosphate buffer at pH 7.4. contained 10 µM Amplex Red® and 1.5 mM H_2O_2 (A). The reaction in 50 mM potassium phosphate buffer at pH 7.4 contained 10 µM Amplex Red® and 1.5 mM H_2O_2 and 1 mM EDTA (B).

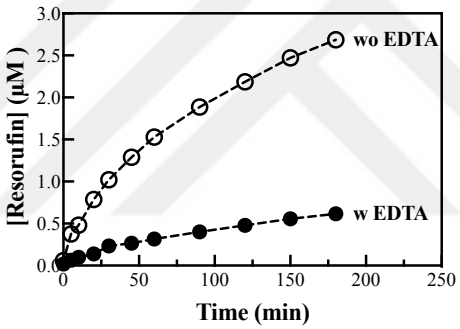

Figure 3.15. Resorufin formation without EDTA was compared to the reaction with addition of 1 mM EDTA in 50 mM potassium phosphate buffer at pH 7.4 with 1.5 mM H_2O_2 as oxidant (●: with EDTA, ○: without EDTA).

Amplex Red® oxidation catalyzed by WT and L69G CYP119 was performed in the presence of 1 mM EDTA at room temperature for 60 min. The reactions contained 1.5 µM enzyme, 10 µM Amplex Red®, 1.5 mM H_2O_2 and 1 mM EDTA in 50 mM potassium phosphate buffer at pH 7.4. Reaction was completed in 20 min as shown in Figure 3.16.C. Concentration of final resorufin was calculated by using extinction coefficient at 570 nm in formula shown section 2.2.9. At the end of the reaction, 7% of Amplex Red® was oxidized by WT and 9% of Amplex Red® was oxidized by L69G CYP119. During the reaction catalyzed by WT CYP119, the heme Soret of WT CYP119

did not decrease significantly. But a decrease in the heme Soret of L69G CYP119 was observed during the reaction (Figure 3.16.B). During the reaction catalyzed by L69G CYP119, H_2O_2 used as an oxidant in the Amplex Red® oxidation caused heme degradation in L69G CYP119.

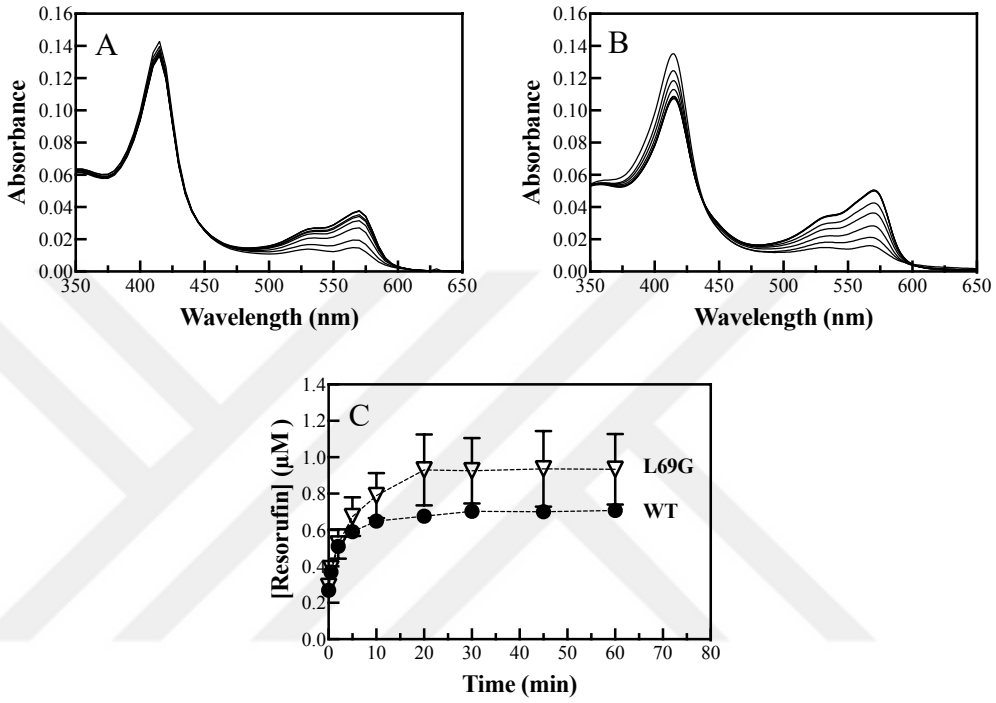

Figure 3.16. UV-Visible spectra of Amplex Red® oxidation by WT CYP119 (A) and L69G CYP119 (B). The spectra were taken at 0, 5, 10, 20, 30, 45 and 60 min. Comparison of resorufin formation by WT CYP119 (●) and L69G CYP119 (▽) (C).

Kinetic analysis of Amplex Red® oxidation by WT and L69G CYP119 was investigated. Amplex Red® reactions were performed with increasing concentration of H_2O_2. Lineweaver-Burk plot is shown for comparison in Figure 3.17. Kinetic parameters were determined by nonlinear fitting of the data to Michealis-Menten equation. There was a little decrease in the K_m and k_{cat} observed in the L69G CYP119 (Table 3.1).

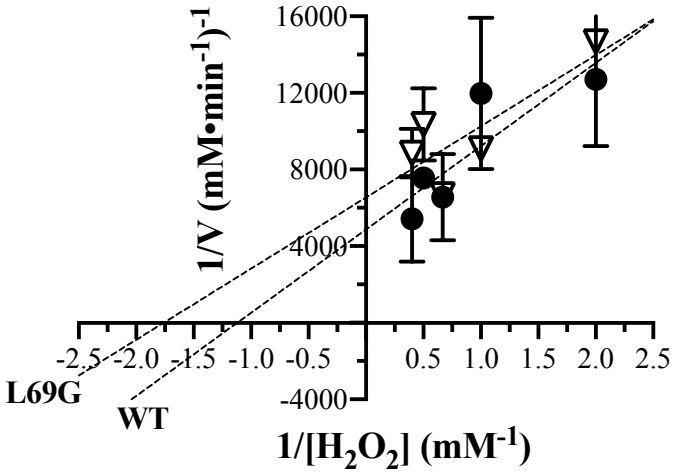

Figure 3.17. Kinetic analysis of Amplex Red® oxidation catalyzed by H_2O_2 by WT CYP119 (●) and L69G CYP119 (▽) using Lineweaver-Burk plot. Amplex Red® oxidation was carried out with 0.5 - 2.5 mM of H_2O_2.

Table 3.1. Kinetic paramters of Amplex Red® oxidation by WT and L69G CYP119.

	K_m (mM)	k_{cat} (× 10^{-3} s^{-1})	V_{max} (× 10^{-3} mM · min^{-1})
WT CYP119	0.82 ± 0.46	2.1 ± 0.3	0.19 ± 0.03
L69G CYP119	0.36 ± 0.29	1.5 ± 0.4	0.14 ± 0.04

3.7.2. Kinetic Analysis of Styrene Epoxidation

Styrene epoxidation activity was studied for activity of WT and L69G CYP119. The styrene epoxidation was carried out in 50 mM potassium phosphate buffer at pH 7.4 at room temperature for 10 min. *tert*-buthyl hydroperoxide (TBHP) was used as oxidant in the reaction. The reaction was analyzed by HPLC. During HPLC analysis UV was followed at 220 nm. First, retention times of styrene and styrene oxide were determined as 6.5 min and 4.27 min, respectively. Styrene oxide was produced as result of the reaction. Concentrations of styrene oxide resulting from the reaction were calculated via calibration curve of styrene oxide. The formation of styrene oxide was followed with variable concentrations of styrene. Lineweaver-Burk plot is shown for comparison in

Figure 3.18. Kinetic parameters were determined by nonlinear fitting of the data to Michealis-Menten equation (Table 3.2). L69G mutation caused about threefold increse in k_{cat} and did not change significantly K_m for styrene.

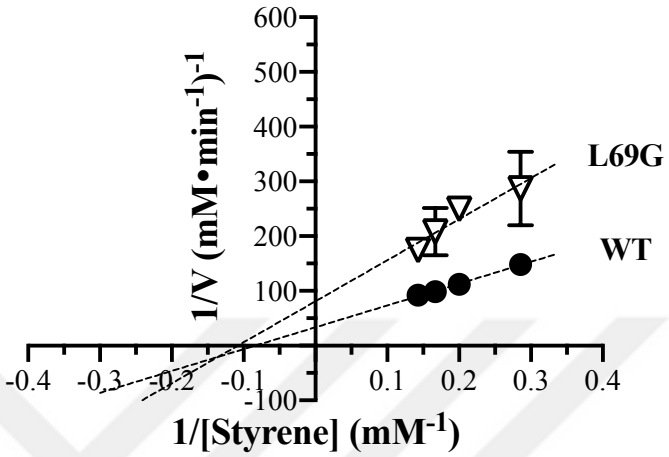

Figure 3.18. Kinetic analysis of styrene epoxidation by different concentrations of styrene (3.5-7 mM) by WT CYP119 (●) and L69G CYP119 (▽) using Lineweaver-Burk plot.

Table 3.2. Kinetic parameters of styrene epoxidation by WT and L69G CYP119.

	K_m (mM)	k_{cat} (s^{-1})	V_{max} (× 10^{-3} mM/min)
WT CYP119	10.6 ± 1.9	0.03 ± 0.01	27.6 ± 3.2
L69G CYP119	17.7 ± 16.4	0.08 ± 0.03	19.5 ± 13.6

3.7.3. Analysis of Progesterone Conversion

Previous computational studies in our laboratories predicted an increase in hydroxylation activity of progesterone by L69G mutation on WT CYP119 (Kestevur Doğru, 2019). Progesterone oxidation catalyzed by L69G and WT CYP119 was investigated. Progesterone oxidation was carried out with three different peroxides H_2O_2, *tert*-buthyl hydroperoxide (TBHP) and cumene hydroperoxide at two different concentrations (1 mM and 10 mM H_2O_2, 3 mM and 7 mM TBHP, 1 mM and 5 mM

cumene hydroperoxide). Thin Layer Chromatography (TLC) was used to monitor hydroxylation of progesterone by L69G CYP119. Spot for product formation was observed as a result of the reaction by L69G CYP119 with 1 mM cumene hydroperoxide while the spot was not observed in the reaction with other oxidants. The product obtained was UV active, since the spot was observed before the TLC plate was sprayed with sulfuric acid (H_2SO_4) (Figure 3.19.A). The reaction with the enzyme was compared to control reaction without the enzyme. The spot of product obtained was not observed in the control reaction. Another product spot which is not UV active was observed in the TLC plate of the reaction by WT CYP119 (Figure 3.20). Progesterone oxidation by L69G and WT CYP119 resulted in different products most likely hydroxylation at different carbons of progesterone was obtained.

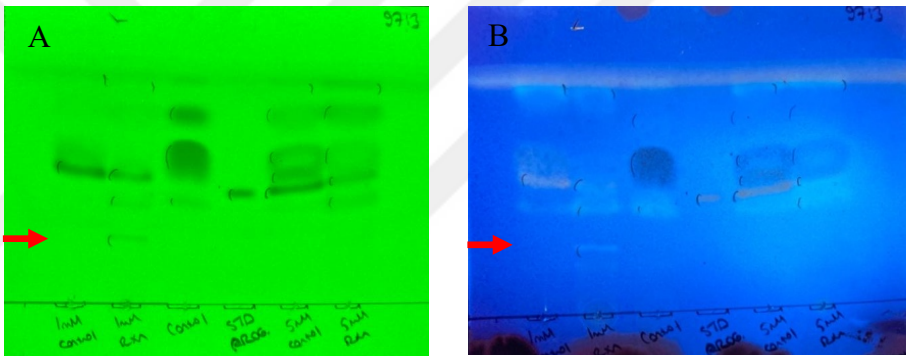

Figure 3.19. TLC plates showing the reactions catalyzed by L69G CYP119 and control reactions (Silica gel 97:3 ($CHCl_3$: MeOH). The plate was displayed under UV (A). Lane 1: The control reaction with 1 mM cumene hydroperoxide. Lane 2: The reaction with 1 mM cumene hydroperoxide. Lane 3: Cumene hydroperoxide. Lane 4: Progesterone. Lane 5: The control reaction with 5 mM cumene hydroperoxide. Lane 6: The reaction with 5 mM cumene hydroperoxide (A). The same plate sprayed with sulfuric acid (H_2SO_4) was displayed under UV (B).

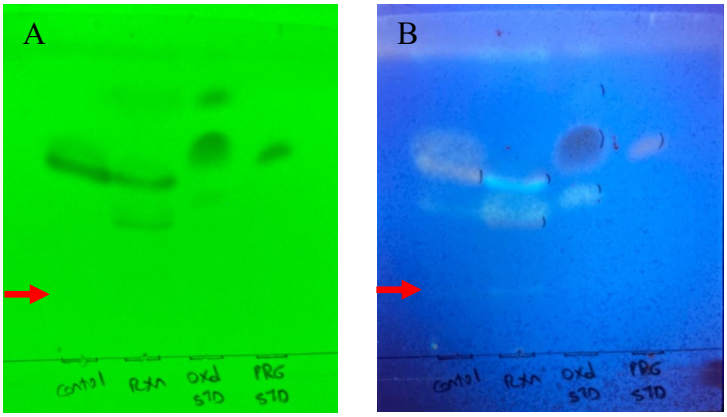

Figure 3.20. TLC plates showing the reactions catalyzed by WT CYP119 and control reactions (Silica gel 97:3 ($CHCl_3$: MeOH). The plate was displayed under UV (A). Lane 1: The control reaction with 1 mM cumene hydroperoxide. Lane 2: The reaction with 1 mM cumene hydroperoxide. Lane 3: Cumene hydroperoxide. Lane 4: Progesterone (A). The same plate sprayed with sulfuric acid (H_2SO_4) was displayed under UV (B).

For HPLC analysis, hydroxylation of progesterone catalyzed by L69G and WT CYP119 was performed adding 1 mM cumene hydroperoxide in 50 mM potassium phosphate buffer at pH 7.4. Reaction products were extracted as described in the Materials and Methods 2.2.10.3 section. For analysis of reaction products, HPLC chromatograms were followed at 254 nm. Retention time of progesterone was determined to be 14.7 min (Figure 3.21) and retention times of cumene hydroperoxide only products were determined at 7.1, 8.3 and 9.2 min (Figure 3.22). A new different peak at 10.4 min (red rectangular) was observed in the presence of L69G CYP119, it is thought to belong to hydroxylated progesterone. This new peak was not observed in the control reaction with no enzyme present and in the reaction by WT CYP119.

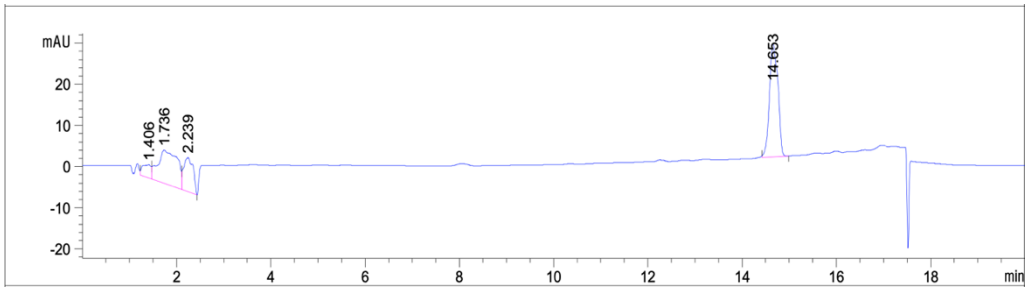

Figure 3.21. HPLC chromatogram of 150 µM progesterone extracted.

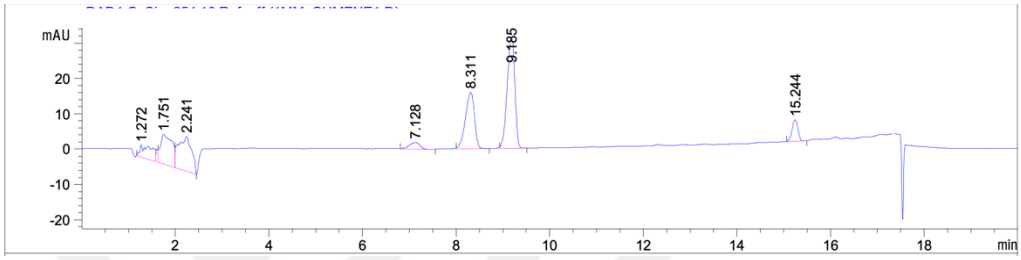

Figure 3.22. HPLC chromatogram of 1 mM cumene hydroperoxide.

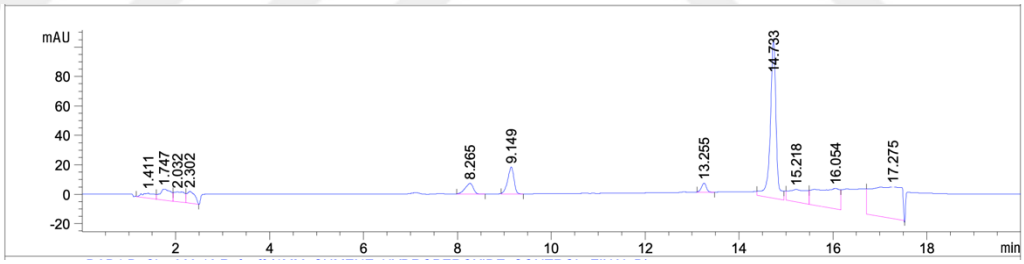

Figure 3.23. HPLC chromatogram of the control reaction without the enzyme. The control reaction contained 150 µM progesterone and 1 mM cumene hydroperoxide in 50 mM potassium phosphate buffer at pH 7.4.

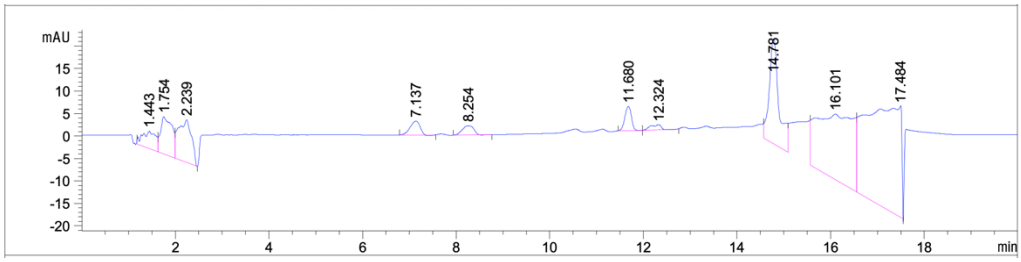

Figure 3.24. HPLC chromatogram of the reaction by WT CYP119. The reaction contained 10 µM WT CYP119, 150 µM progesterone and 1 mM cumene hydroperoxide in 50 mM potassium phosphate buffer at pH 7.4.

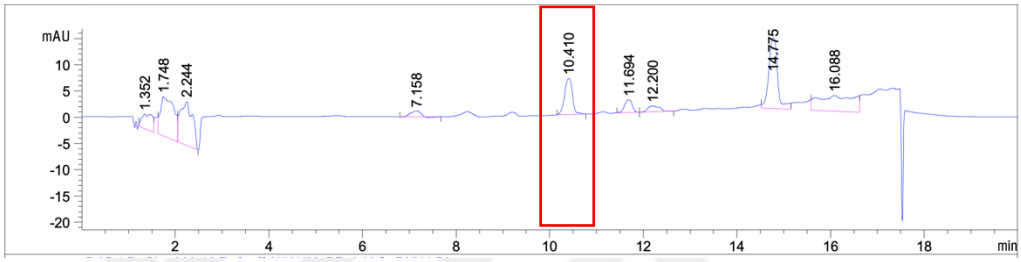

Figure 3.25. HPLC chromatogram of the reaction by L69G CYP119. The reaction contained 10 µM L69G CYP119, 150 µM progesterone and 1 mM cumene hydroperoxide in 50 mM potassium phosphate buffer at pH 7.4.

3.7.3.1 Identification of Products Formed in Oxidation of Progesterone Catalyzed by L69G CYP119

The novel product obtained from the reaction catalyzed by L69G CYP119 detected at 10.41 min was manually collected by out of HPLC UV detector and evaporated for Mass Spectrometry analysis. The isolated product was analyzed by HPLC after dissolving in the methanol to control isolation (Figure 3.26). Then, changes in mass spectra of the the product from progesterone was analyzed using Matrix-assisted Laser Desorption/Ionization Time-of-Flight /Time-of-Flight (MALDI-TOF/TOF) (Figure 3.27). Progesterone extracted and treated with the same methods were used as control. Mass spectra of progesterone showed m/z 315.07 which corresponds to molecular weight of progesterone. For hydroxylated progesterone, there was very small peak at m/z 315.04

and new peak with m/z 371.33 was observed. While the expected m/z 331 for hydroxyprogesterone was not observed. The new peak at m/z 371.33 can be a common acetonitrile adduct, [M+H+ACN]+ for the hydroxylated product.

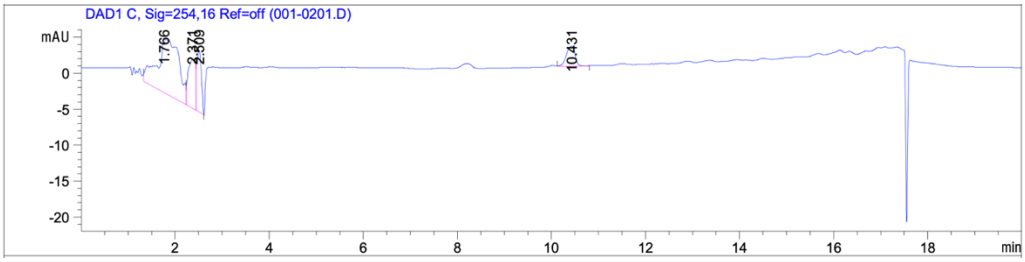

Figure 3.26. HPLC chromatogram of the product obtained from the reaction by L69G CYP119.

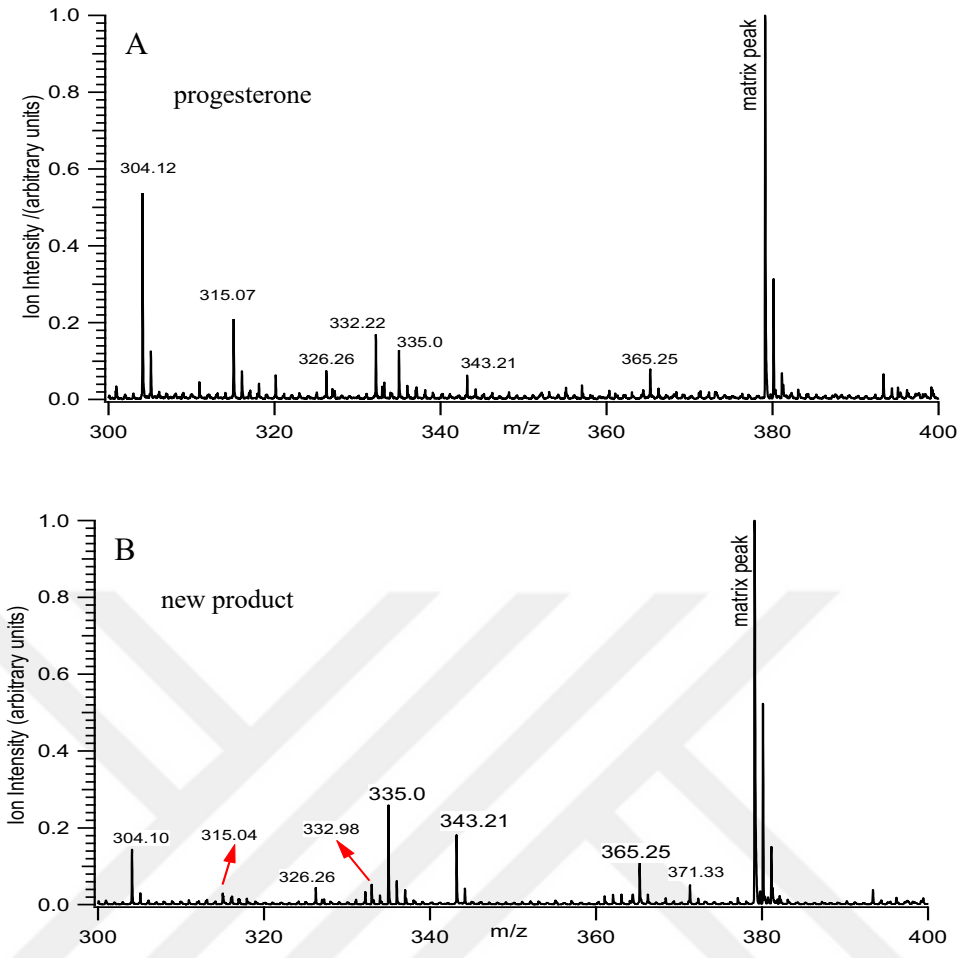

Figure 3.27. MALDI-TOF/TOF chromatograms of hydroxylated progesterone (A) and progesterone (B).

3.7.3.2 Investigation of Kinetics of Progesterone Oxidation Catalyzed by L69G Mutant

Progesterone oxidation catalyzed by L69G CYP119 were performed under variable conditions. Also, the reactions with 150 µM progesterone was followed at 5, 10, 30 and 60 min. For kinetic analysis of conversion of progesterone to product (most likely hydroxylated progesterone), integration area of the peak at 10.41 min described above was plotted against concentration of progesterone (Figure 3.28.A) and time (Figure 3.28.B). After 30 min, integration area of product was constant.

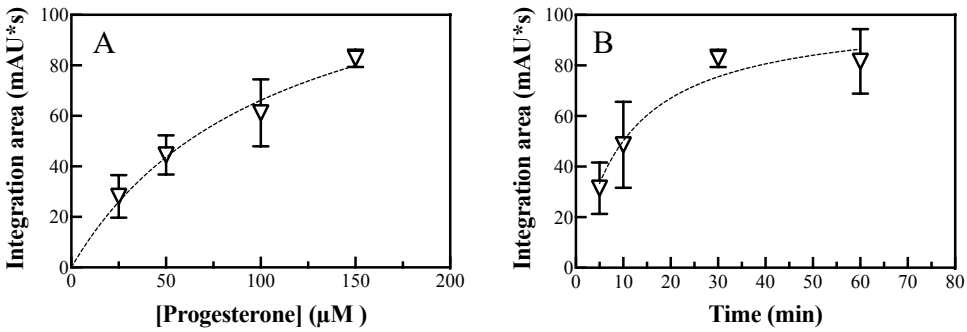

Figure 3.28. Analysis of conversion of progesterone to hydroxylated progesterone by L69G CYP119 with different concentrations of progesterone (50-150 µM) (A) and by the time (B).

3.8. Results of Reactions of WT and L69G Mutant CYP119 with Peroxides

Reactions with peroxides containing hydrogen peroxide (H_2O_2), *tert*-buthyl hydroperoxide and cumene hydroperoxide were studied as mentioned methods part section.

3.8.1. Reactions of WT and L69G Mutant CYP119 with Hydrogen peroxide

The reaction of H_2O_2 with WT and L69G CYP119 was studied at room temperature. The reaction contained 1.5 mM H_2O_2, 1.5 µM enzyme and 1 mM EDTA. The Soret absorbance at 414 nm changes significantly during the reaction for both WT and L69G CYP119 as shown in Figure 3.C. L69G CYP119 has a lower stability towards degradation by H_2O_2 than WT CYP119. Superoxide forms during the reaction with hydrogen peroxide. Superoxide production causes heme degradation (Nagababu & Rifkind, 2000). The Soret absorbance at 414 nm was followed for heme degradation. During the reaction the Soret absorbance of WT and L69G CYP119 decreased by 15% and 29%, respectively. The observed rate constant for the decrease in Soret absorbance

of WT CYP119 was $1.8 \pm 0.6 \times 10^{-3}$ s^{-1} and the observed rate constant for the decrease in Soret absorbance of L69G CYP119 was $7.8 \pm 1.8 \times 10^{-3}$ s^{-1}. The rate of decrease in Soret absorbance of L69G CYP119 was faster than the Soret absorbance of WT CYP119.

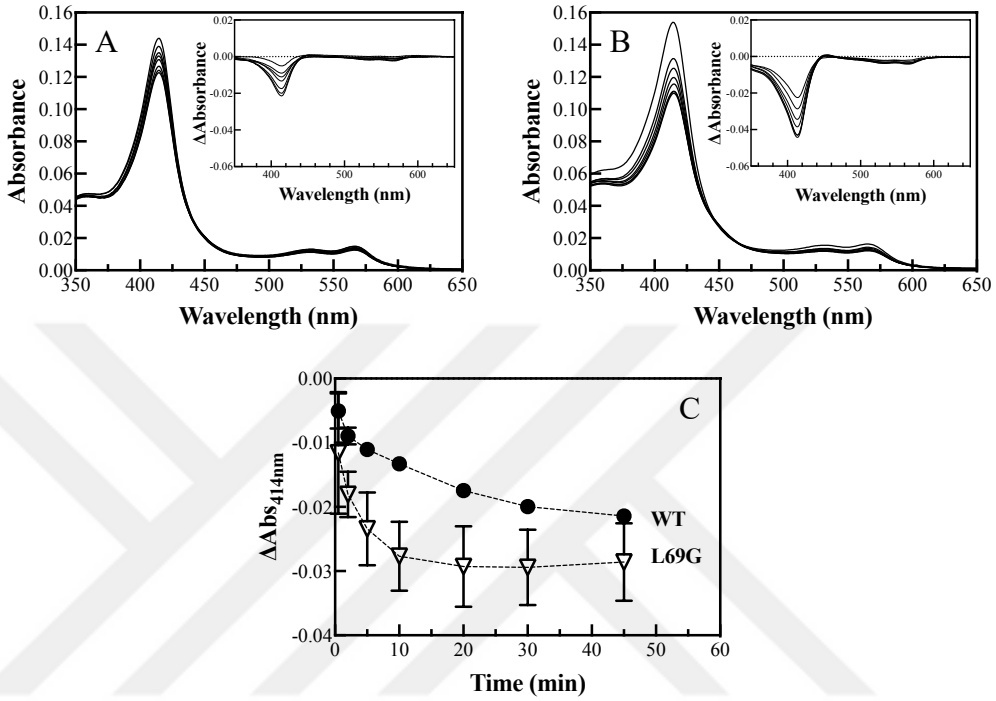

Figure 3.29. Changes in the spectra of H_2O_2 reaction with WT CYP119 (A) and L69G CYP119 (B). The spectra analysis was at 0, 2, 5, 10, 20, 30 and 45 min. Insets demonstrate difference spectra. Comparison of the decrease in 414 nm of WT CYP119 (●) and L69G CYP119 (▽) (C).

3.8.2. Reactions of WT and L69G Mutant CYP119 with *tert*-butyl hydroperoxide

The reaction of *tert*-butyl hydroperoxide (TBHP) with WT and L69G CYP119 was studied at room temperature. The reaction contained 7 mM (TBHP) and 1.5 µM enzyme in 50 mM potassium phosphate buffer at pH 7.4. Superoxide forms during the reaction with *tert*-butyl hydroperoxide (TBHP). Heme degradation occurs due to superoxide production (Nagababu & Rifkind, 2000). The Soret absorbance at 414 nm

was followed for heme degradation. The rate of decrease in Soret absorbance of WT CYP119 was faster than the Soret absorbance of L69G CYP119. The Soret absorbance at 414 nm changes significantly during the reaction for WT CYP119 as shown in Figure 3.21.C. L69G CYP119 has a higher stability to *tert*-butyl hydroperoxide than WT CYP119. During the reaction the Soret absorbance of WT and L69G CYP119 decreased by 63% and 13%, respectively. The observed rate constant for the decrease in Soret absorbance of WT CYP119 was $1.8 \pm 0.5 \times 10^{-3}$ s^{-1} and the observed rate constant for the decrease in Soret absorbance of L69G CYP119 was $0.14 \pm 0.08 \times 10^{-3}$ s^{-1}.

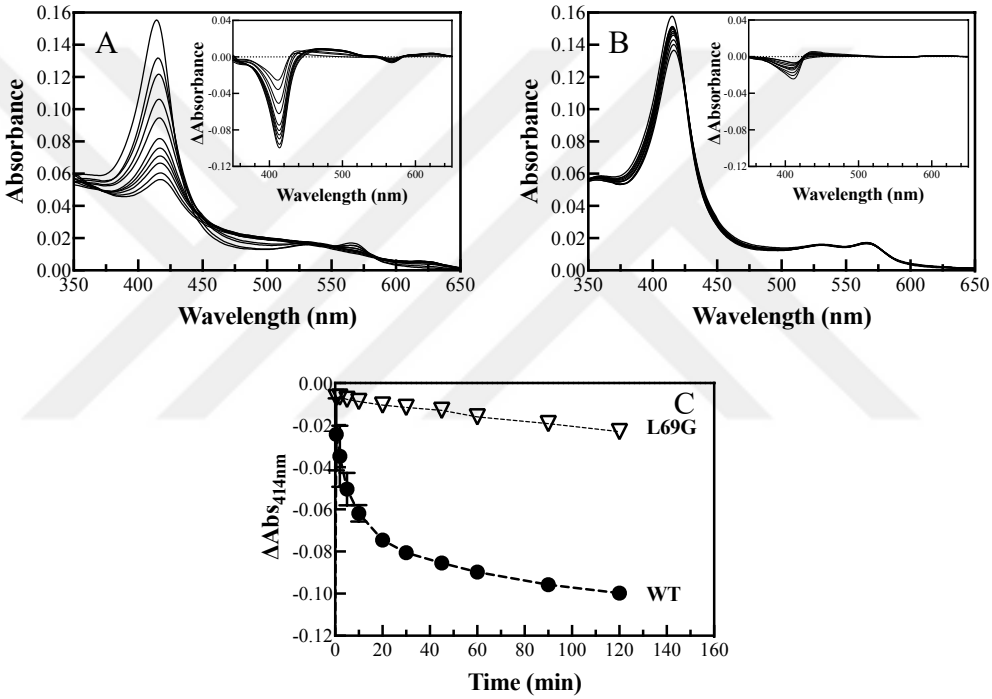

Figure 3.30. Changes in the spectra of *tert*-butyl hydroperoxide reaction with WT CYP119 (A) and L69G CYP119 (B). The spectra analysis was at 0, 2, 5, 10, 20, 30, 45, 60, 90 and 120 min. Insets demonstrate difference spectra. Comparison of the decrease in 414 nm of WT CYP119 (●) and L69G CYP119 (▽) (C).

3.8.3. Reactions of WT and L69G Mutant CYP119 with Cumene Hydroperoxide

The reaction of cumene hydroperoxide (CHP) with WT and L69G CYP119 was studied at room temperature. The reaction contained 1 mM cumene hydroperoxide and 1.5 μM enzyme in 50 mM potassium phosphate buffer at pH 7.4. Superoxide forms during the reaction with cumene hydroperoxide. Heme degradation occurs due to superoxide production during the reaction (Nagababu & Rifkind, 2000). The Soret absorbance at 414 nm was followed for heme degradation. The Soret absorbance at 414 nm changes significantly during the reaction for both WT and L69G CYP119 as shown in Figure 3.C. L69G CYP119 has a higher stability to cumene hydroperoxide than WT CYP119. The rate of decrease in Soret absorbance of WT CYP119 was faster than the Soret absorbance of L69G CYP119. During the reaction the Soret absorbance of WT and L69G CYP119 decreased by 50% and 68%, respectively. The observed rate constant for the decrease in Soret absorbance of WT CYP119 was $38 \pm 2.8 \times 10^{-3}$ s^{-1} and the observed rate constant for the decrease in Soret absorbance of L69G CYP119 was $0.5 \pm 0.1 \times 10^{-3}$ s^{-1}.

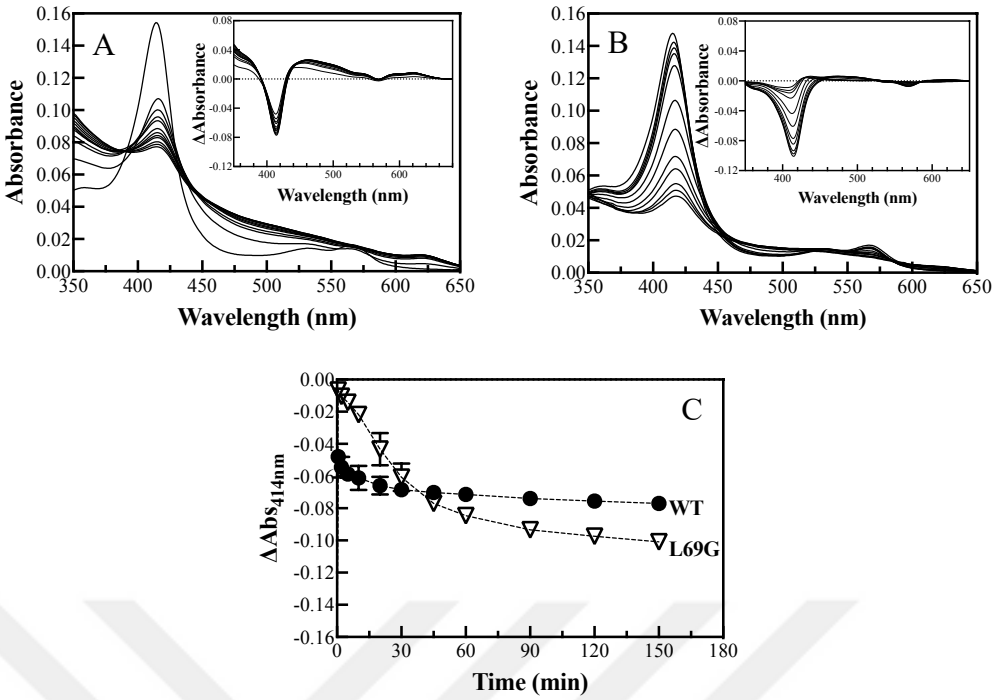

Figure 3.31. Changes in the spectra of cumene hydroperoxide reaction with WT CYP119 (A) and L69G CYP119 (B). The spectra analysis was at 0, 2, 5, 10, 20, 30, 45, 60, 90, 120 and 150 min. Insets demonstrate difference spectra. Comparison of the decrease in 414 nm of WT CYP119 (●) and L69G CYP119 (▽) (C).

CHAPTER 4

CONCLUSION

Hydroxylated progesterone derivatives are significant for biopharmaceutical industry. The thermoacidophilic CYP119 is an important biocatalyst. This project aimed at expression and purification of L69G and WT CYP119 and conversion of progesterone to hydroxylated progesterone derivatives by L69G CYP119.

Amplex Red® oxidation of L69G and WT CYP119 were also investigated by using H_2O_2 as an oxidant. The results of oxidation by the enzyme demonstrated that the activity of L69G CYP119 is similar to WT CYP119. L69G CYP119 showed a lower stability towards degradation by H_2O_2 than WT CYP119 in the absence of substrate.

Styrene epoxidation by L69G and WT CYP119 were performed with TBHP as an oxidant. L69G mutation caused a decrease in the activity for styrene epoxidation. L69G CYP119 showed higher stability towards TBHP-dependent degradation compared with WT CYP119.

L69G mutation on WT CYP119 caused higher specificity to progesterone binding. Progesterone hydroxylation by L69G CYP119 was studied with cumene hydroperoxide as an oxidant to produce hydroxylated progesterone derivatives. A new product, was UV active, was observed in chromatogram of HPLC with different products from progesterone hydroxylation by WT CYP119 under the same conditions. Little difference between the mass spectra of the new product, thought to be hydroxylated progesterone, and progesterone was observed as result of MALDI-TOF/TOF analysis. Heme of WT CYP119 was degraded quickly by cumene hydroperoxide compared with L69G CYP119.

This study will contribute to efficient and rapid production of progesterone derivatives for drug synthesis and provide information about effect of L69G mutation on CYP119 structure and its catalytic activity on different substrates.

REFERENCES

Aslantas, Y., & Surmeli, N. B. (2019). Effects of N-Terminal and C-Terminal Polyhistidine Tag on the Stability and Function of the Thermophilic P450 CYP119. *Bioinorganic Chemistry and Applications*, *2019*, 8080697. https://doi.org/10.1155/2019/8080697

Aslantaş, Y. (2018). *Optimization of expression and isolation of a thermophilic P450 enzyme*. http://openaccess.iyte.edu.tr/xmlui/handle/11147/7209

Bernhardt, R., & Urlacher, V. B. (2014). Cytochromes P450 as promising catalysts for biotechnological application: Chances and limitations. *Applied Microbiology and Biotechnology*, *98*(14), 6185-6203. https://doi.org/10.1007/s00253-014-5767-7

Blair, E., Greaves, J., & Farmer, P. J. (2004). High-temperature electrocatalysis using thermophilic P450 CYP119: Dehalogenation of CCl4 to CH4. *Journal of the American Chemical Society*, *126*(28), 8632-8633. https://doi.org/10.1021/ja0488333

Bommarius, A. S., & Paye, M. F. (2013). Stabilizing biocatalysts. *Chemical Society Reviews*, *42*(15), 6534-6565. https://doi.org/10.1039/c3cs60137d

Chen, R. (2001). Enzyme engineering: Rational redesign versus directed evolution. *Trends in Biotechnology*, *19*(1), 13-14. https://doi.org/10.1016/s0167-7799(00)01522-5

Cirino, P. C., & Arnold, F. H. (2002). Regioselectivity and Activity of Cytochrome P450 BM-3 and Mutant F87A in Reactions Driven by Hydrogen Peroxide. *Advanced Synthesis & Catalysis*, *344*(9), 932-937. https://doi.org/10.1002/1615-4169(200210)344:9<932::AID-ADSC932>3.0.CO;2-M

Cook, D. J., Finnigan, J. D., Cook, K., Black, G. W., & Charnock, S. J. (2016). Cytochromes P450: History, Classes, Catalytic Mechanism, and Industrial Application. *Advances in Protein Chemistry and Structural Biology*, *105*, 105-126. https://doi.org/10.1016/bs.apcsb.2016.07.003

Di Renzo, G. C., Tosto, V., & Tsibizova, V. (2020). Progesterone: History, facts, and artifacts. *Best Practice & Research Clinical Obstetrics & Gynaecology*, *69*, 2-12. https://doi.org/10.1016/j.bpobgyn.2020.07.012

Guengerich, F. P. (2002). Cytochrome p450 enzymes in the generation of commercial products. *Nature Reviews Drug Discovery*, *1*(5), 359-366. https://doi.org/10.1038/nrd792

Hrycay, E. G., & Bandiera, S. M. (2012). The monooxygenase, peroxidase, and peroxygenase properties of cytochrome P450. *Archives of Biochemistry and Biophysics*, *522*(2), 71-89. https://doi.org/10.1016/j.abb.2012.01.003

Immoos, C. E., Chou, J., Bayachou, M., Blair, E., Greaves, J., & Farmer, P. J. (2004). Electrocatalytic reductions of nitrite, nitric oxide, and nitrous oxide by thermophilic cytochrome P450 CYP119 in film-modified electrodes and an analytical comparison of its catalytic activities with myoglobin. *Journal of the American Chemical Society*, *126*(15), 4934-4942. https://doi.org/10.1021/ja038925c

Kestevur Doğru, E. (2019). *Bioinformatics based approach to design a thermophilic P450 fot industrial biocatalysis*. http://openaccess.iyte.edu.tr/xmlui/handle/11147/9679

Koo, L. S., Tschirret-Guth, R. A., Straub, W. E., Moënne-Loccoz, P., Loehr, T. M., & Ortiz de Montellano, P. R. (2000). The active site of the thermophilic CYP119 from Sulfolobus solfataricus. *The Journal of Biological Chemistry*, *275*(19), 14112-14123. https://doi.org/10.1074/jbc.275.19.14112

Koo, Laura S., Immoos, C. E., Cohen, M. S., Farmer, P. J., & Ortiz de Montellano, P. R. (2002). Enhanced electron transfer and lauric acid hydroxylation by site-directed mutagenesis of CYP119. *Journal of the American Chemical Society*, *124*(20), 5684-5691. https://doi.org/10.1021/ja017174g

Li, Z., Jiang, Y., Guengerich, F. P., Ma, L., Li, S., & Zhang, W. (2020). Engineering cytochrome P450 enzyme systems for biomedical and biotechnological applications. *The Journal of Biological Chemistry*, *295*(3), 833-849. https://doi.org/10.1074/jbc.REV119.008758

Lopata, A., Jójárt, B., Surányi, É. V., Takács, E., Bezúr, L., Leveles, I., Bendes, Á. Á., Viskolcz, B., Vértessy, B. G., & Tóth, J. (2019). Beyond Chelation: EDTA Tightly Binds Taq DNA Polymerase, MutT and dUTPase and Directly Inhibits dNTPase Activity. *Biomolecules*, *9*(10). https://doi.org/10.3390/biom9100621

McLean, M. A., Maves, S. A., Weiss, K. E., Krepich, S., & Sligar, S. G. (1998). Characterization of a cytochrome P450 from the acidothermophilic archaea Sulfolobus solfataricus. *Biochemical and Biophysical Research*

Communications, *252*(1), 166-172. https://doi.org/10.1006/bbrc.1998.9584

Mondal, A., Das, M., & Mazumdar, S. (2019). Substitution of iron with cobalt in the prosthetic group of bacterial cytochrome P450: Effects on the stability and structure of the protein. *Inorganica Chimica Acta*, *487*, 398-404. https://doi.org/10.1016/j.ica.2018.12.043

Nagababu, E., & Rifkind, J. M. (2000). Reaction of Hydrogen Peroxide with Ferrylhemoglobin: Superoxide Production and Heme Degradation. *Biochemistry*, *39*(40), 12503-12511. https://doi.org/10.1021/bi992170y

Nienhaus, K., & Nienhaus, G. U. (2005). Probing heme protein-ligand interactions by UV/visible absorption spectroscopy. *Methods in Molecular Biology (Clifton, N.J.)*, *305*, 215-242. https://doi.org/10.1385/1-59259-912-5:215

Nikolaus, J., Nguyen, K. T., Virus, C., Riehm, J. L., Hutter, M., & Bernhardt, R. (2017). Engineering of CYP106A2 for steroid 9α- and 6β-hydroxylation. *Steroids*, *120*, 41-48. https://doi.org/10.1016/j.steroids.2017.01.005

O'Reilly, E., Köhler, V., Flitsch, S. L., & Turner, N. J. (2011). Cytochromes P450 as useful biocatalysts: Addressing the limitations. *Chemical Communications (Cambridge, England)*, *47*(9), 2490-2501. https://doi.org/10.1039/c0cc03165h

Puchkaev, A. V., Koo, L. S., & Ortiz de Montellano, P. R. (2003). Aromatic stacking as a determinant of the thermal stability of CYP119 from Sulfolobus solfataricus. *Archives of Biochemistry and Biophysics*, *409*(1), 52-58. https://doi.org/10.1016/s0003-9861(02)00402-2

Puchkaev, A. V., Wakagi, T., & Ortiz de Montellano, P. R. (2002). CYP119 plus a Sulfolobus tokodaii strain 7 ferredoxin and 2-oxoacid:ferredoxin oxidoreductase constitute a high-temperature cytochrome P450 catalytic system. *Journal of the American Chemical Society*, *124*(43), 12682-12683. https://doi.org/10.1021/ja0282036

Rabe, K. S., Kiko, K., & Niemeyer, C. M. (2008). Characterization of the peroxidase activity of CYP119, a thermostable P450 from Sulfolobus acidocaldarius. *Chembiochem: A European Journal of Chemical Biology*, *9*(3), 420-425. https://doi.org/10.1002/cbic.200700450

Sakaki, T. (2012). Practical application of cytochrome P450. *Biological & Pharmaceutical Bulletin*, *35*(6), 844-849. https://doi.org/10.1248/bpb.35.844

Schulz, S., Girhard, M., & Urlacher, V. (2012). Biocatalysis: Key to Selective Oxidations. *ChemCatChem*, *4*, 1889-1895. https://doi.org/10.1002/cctc.201200533

Sheldon, R. A., & Woodley, J. M. (2018). Role of Biocatalysis in Sustainable Chemistry. *Chemical Reviews*, *118*(2), 801-838. https://doi.org/10.1021/acs.chemrev.7b00203

Shoji, O., & Watanabe, Y. (2014). Peroxygenase reactions catalyzed by cytochromes P450. *JBIC Journal of Biological Inorganic Chemistry*, *19*(4), 529-539. https://doi.org/10.1007/s00775-014-1106-9

Sundström-Poromaa, I., Comasco, E., Sumner, R., & Luders, E. (2020). Progesterone – Friend or foe? *Frontiers in Neuroendocrinology*, *59*, 100856. https://doi.org/10.1016/j.yfrne.2020.100856

Suzuki, R., Hirakawa, H., & Nagamune, T. (2014). Electron donation to an archaeal cytochrome P450 is enhanced by PCNA-mediated selective complex formation with foreign redox proteins. *Biotechnology Journal*, *9*(12), 1573-1581. https://doi.org/10.1002/biot.201400007

Szaleniec, M., Wojtkiewicz, A. M., Bernhardt, R., Borowski, T., & Donova, M. (2018). Bacterial steroid hydroxylases: Enzyme classes, their functions and comparison of their catalytic mechanisms. *Applied Microbiology and Biotechnology*, *102*(19), 8153-8171. https://doi.org/10.1007/s00253-018-9239-3

Truppo, M. D. (2017). Biocatalysis in the Pharmaceutical Industry: The Need for Speed. *ACS Medicinal Chemistry Letters*, *8*(5), 476-480. https://doi.org/10.1021/acsmedchemlett.7b00114

Watanabe, I., Nara, F., & Serizawa, N. (1995). Cloning, characterization and expression of the gene encoding cytochrome P-450sca-2 from Streptomyces carbophilus involved in production of pravastatin, a specific HMG-CoA reductase inhibitor. *Gene*, *163*(1), 81-85. https://doi.org/10.1016/0378-1119(95)00394-l

Zhang, C., Li, J., Yang, B., He, F., Yang, S.-Y., Yu, X.-Q., & Wang, Q. (2014). Enhanced turnover rate and enantioselectivity in the asymmetric epoxidation of styrene by new T213G mutants of CYP 119. *RSC Advances*, *4*(52), 27526-27531. https://doi.org/10.1039/C4RA04626A